Electronic Supplementary Information (ESI) for

Single-molecule magnet behaviour and catalytic properties of tetrahedral Co(II) complexes bearing chloride and 1,2-disubstituted benzimidazole as ligands

Jorge Luiz Sônego Milani,*[a,b] Álvaro Farias Arruda da Mata,[a] Igor Santos Oliveira,[a] Ana Karoline Silva Mendanha Valdo,[a] Felipe Terra Martins,[a] Renato Rabelo,[c] Danielle Cangussu,[a] Joan Cano,*[c] Francesc Lloret,[c] Miguel Julve,[c] Rafael Pavão das Chagas*[a]

[a] Instituto de Química, Universidade Federal de Goiás – UFG, Goiânia – GO, Brazil

[b] Departamento de Química, Universidade Federal de Juiz de Fora – UFJF, Juiz de Fora – MG, Brazil

[c] Universitat de València, Departament de Química Inorgánica/Instituto de Ciencia Molecular (ICMol), Paterna (València), Spain

*Corresponding Authors: J. L. S. Milani – e-mail: jorge.milani@ufjf.edu.br
J. Cano – e-mail: joan.cano@uv.es
R. P. das Chagas – e-mail: rpchagas@ufg.br

Table of Contents

1. Compounds characterisation

1.1. ^{1}H and ^{13}C NMR spectra

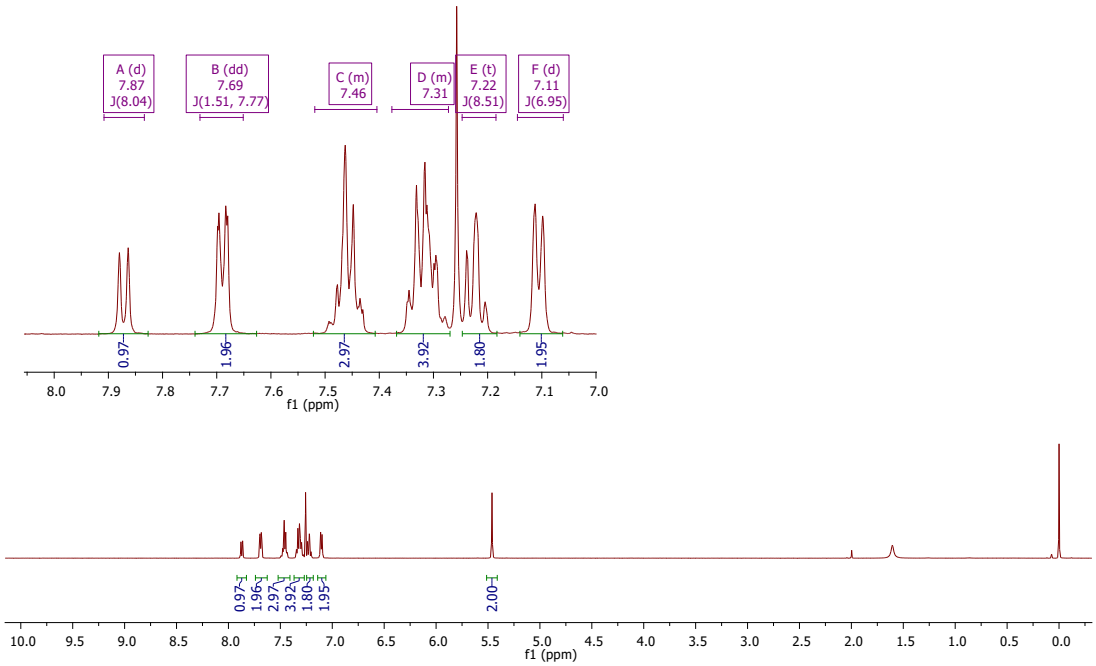

Figure S1. ^{1}H NMR spectra of **L^{1}** in $CDCl_3$.

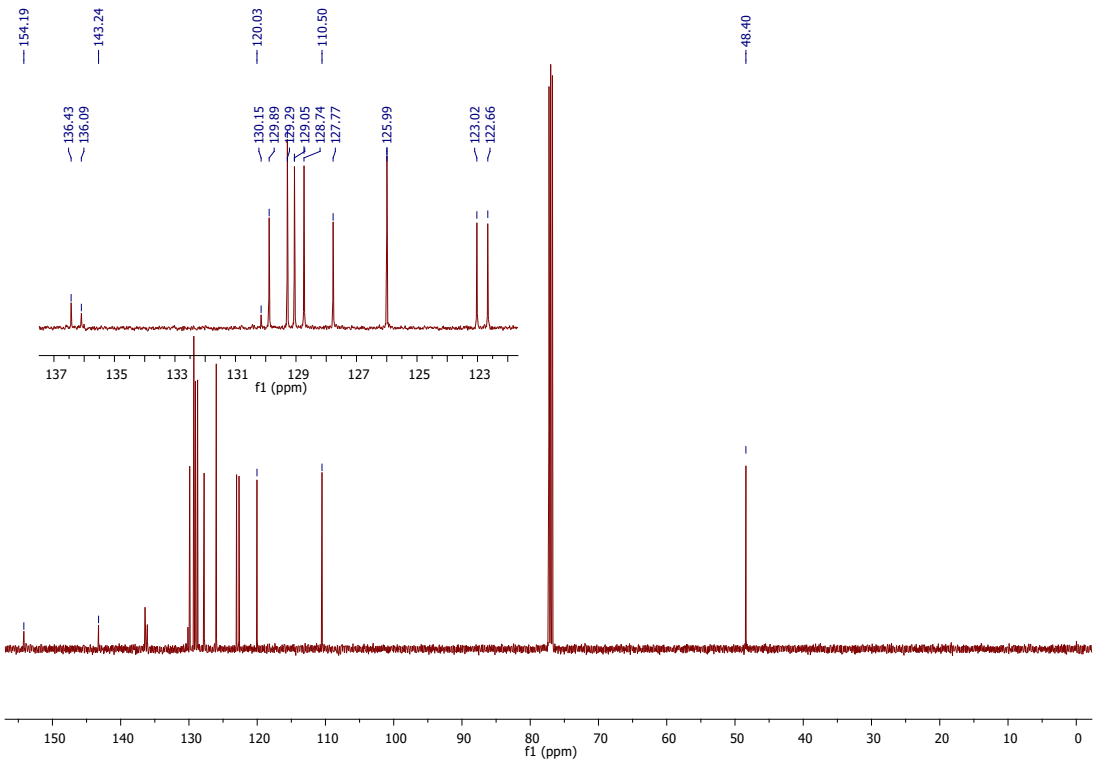

Figure S2. ^{13}C NMR spectra of **L¹** in $CDCl_3$.

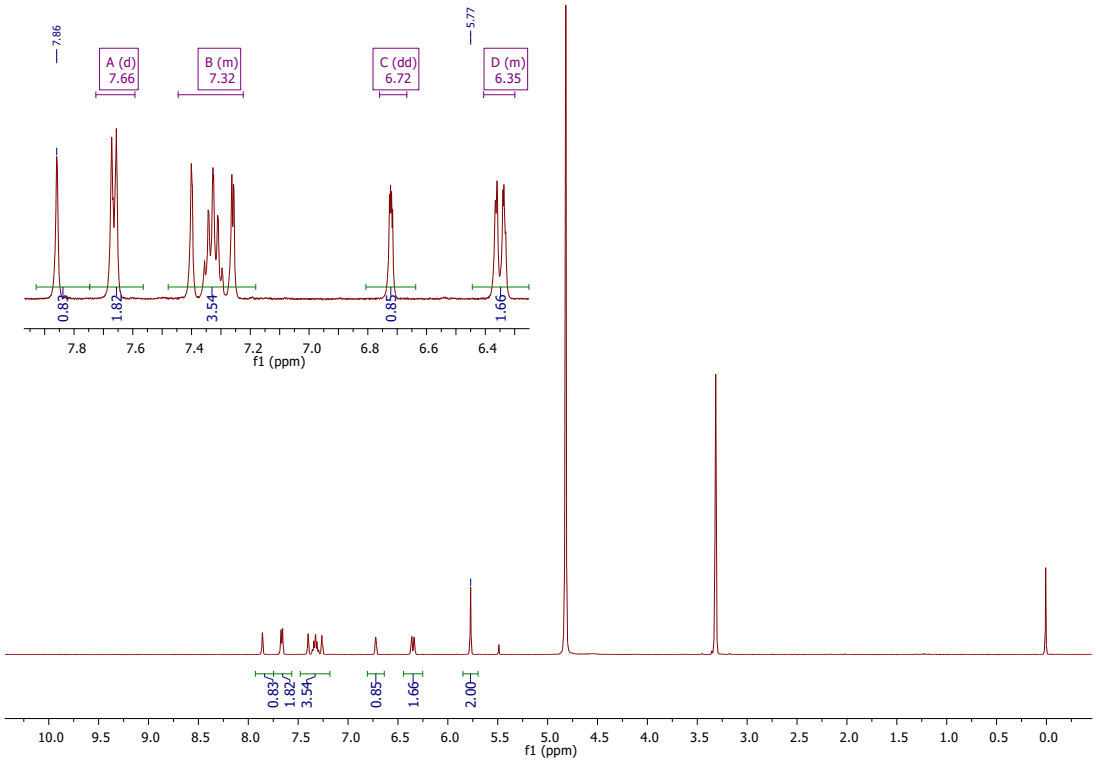

Figure S3. ^{1}H NMR spectra of **L²** in CD_3OD.

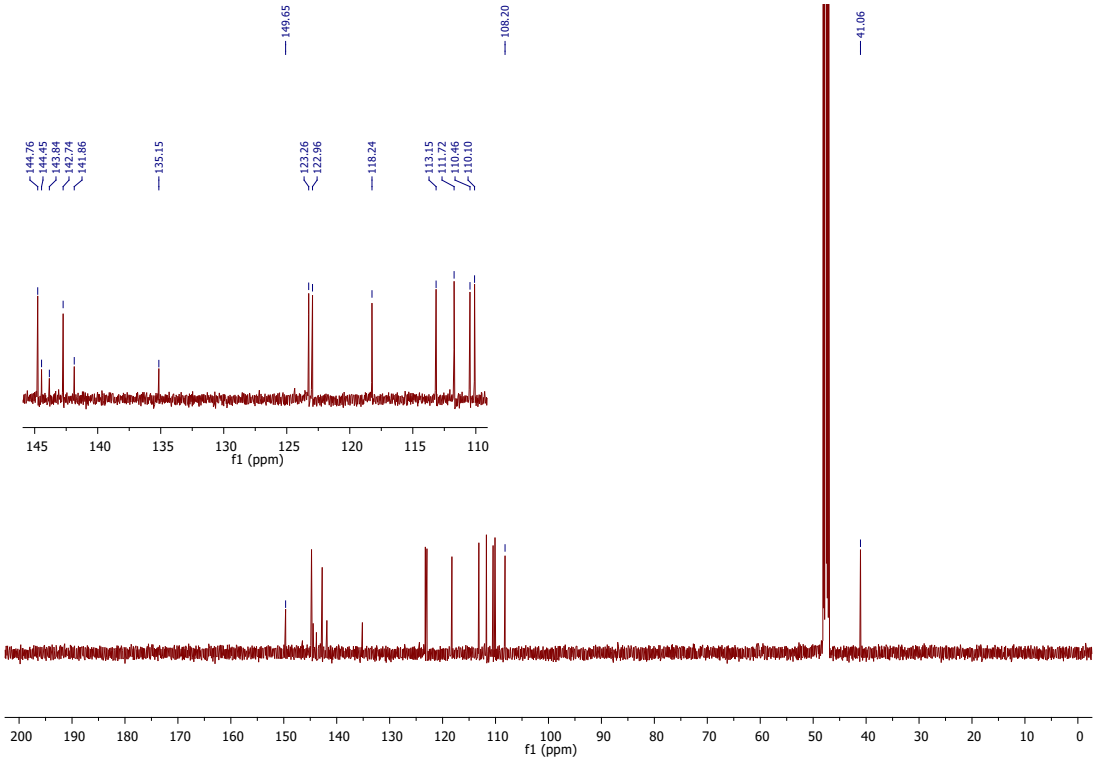

Figure S4. ^{13}C NMR spectra of **L²** in CD_3OD.

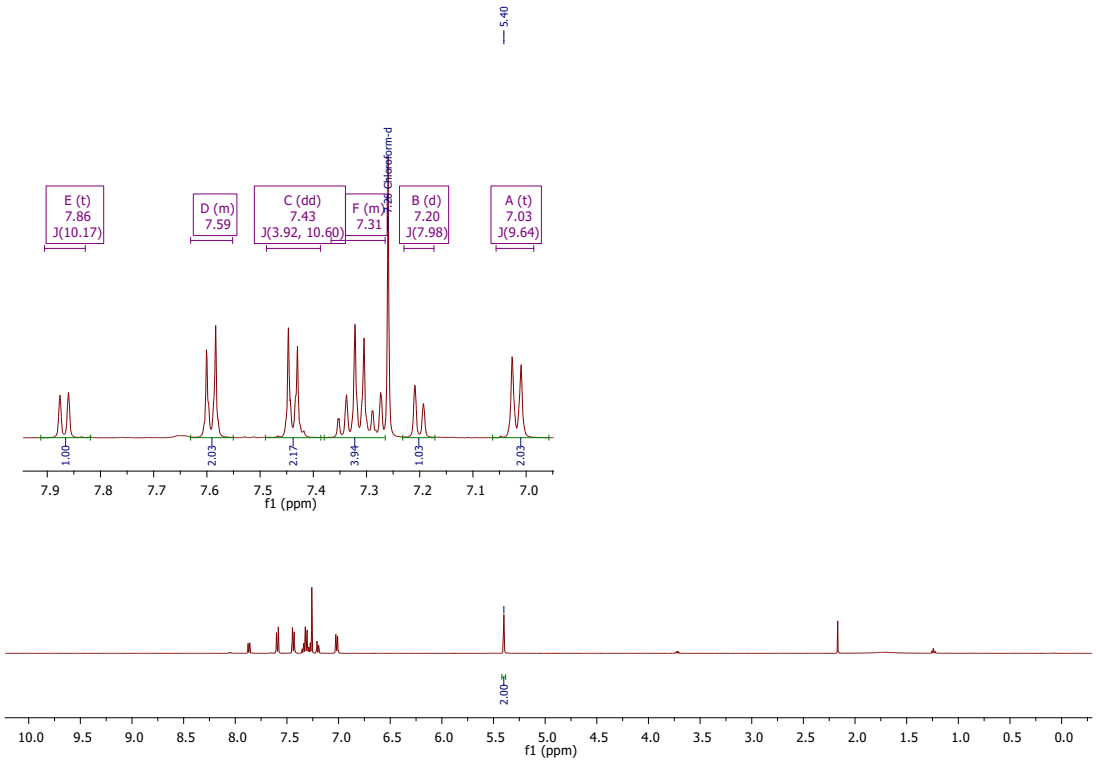

Figure S5. ^{1}H NMR spectra of **L^{3}** in $CDCl_3$.

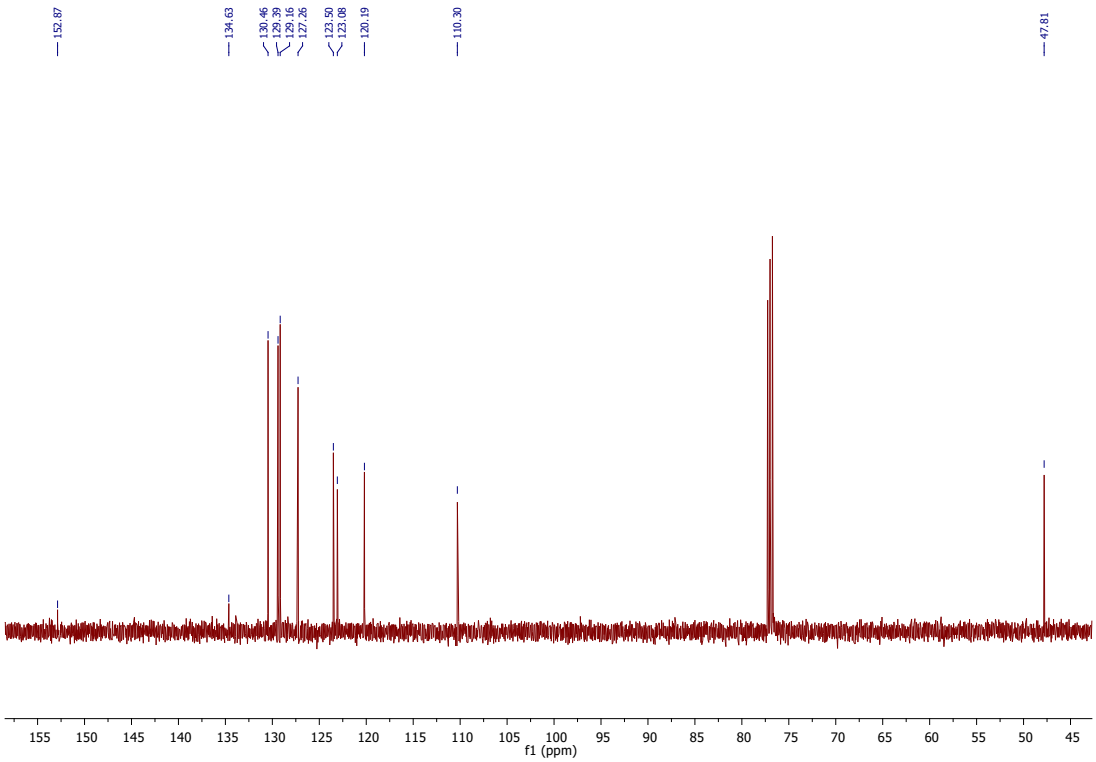

Figure S6. ^{13}C NMR spectra of **L^{3}** in $CDCl_3$.

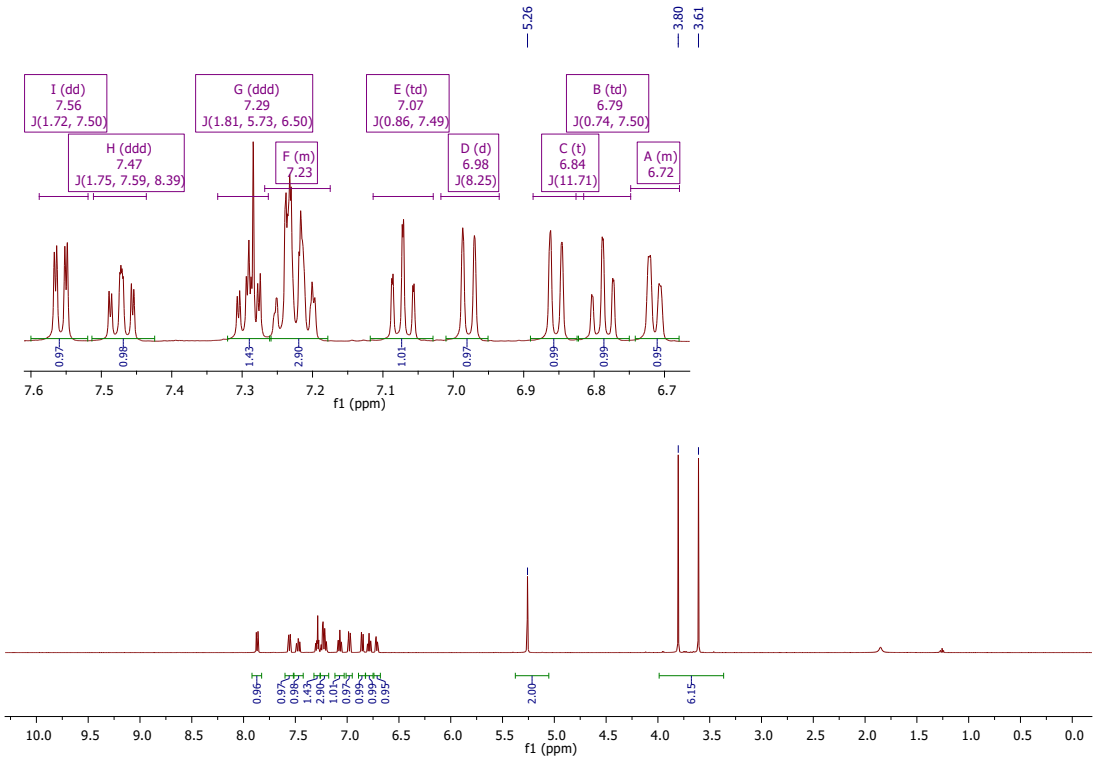

Figure S7. ^{1}H NMR spectra of **L^{4}** in $CDCl_3$.

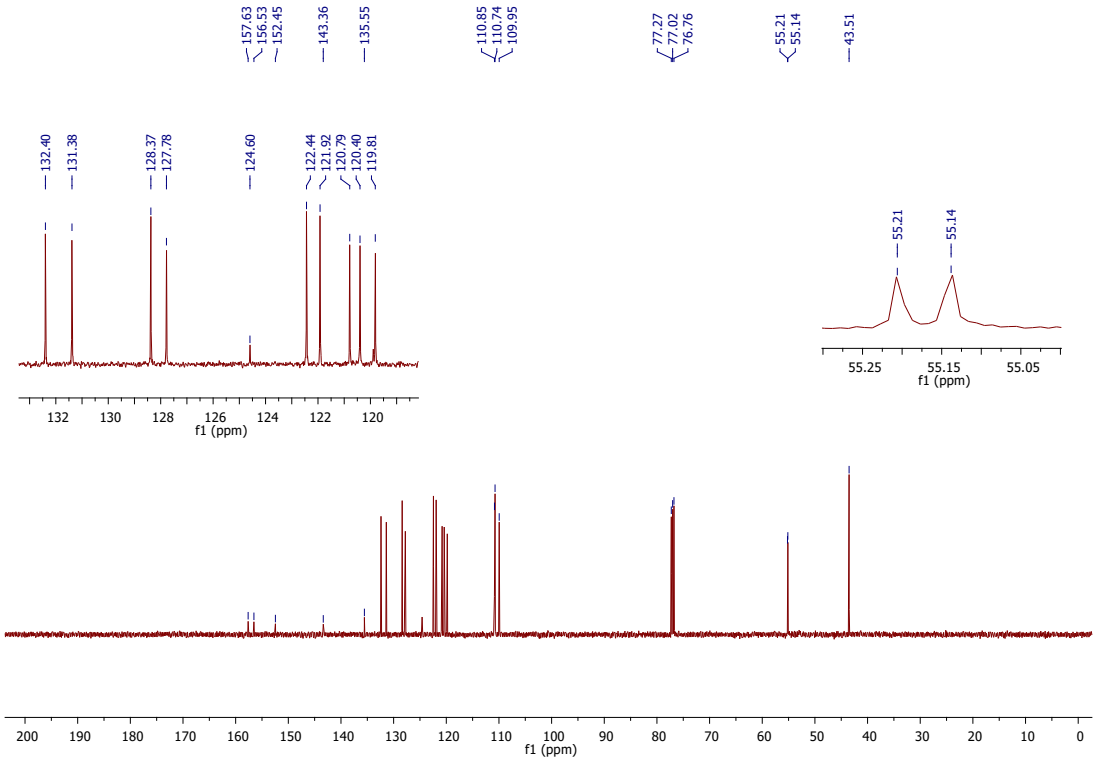

Figure S8. ^{13}C NMR spectra of **L^{4}** in $CDCl_3$.

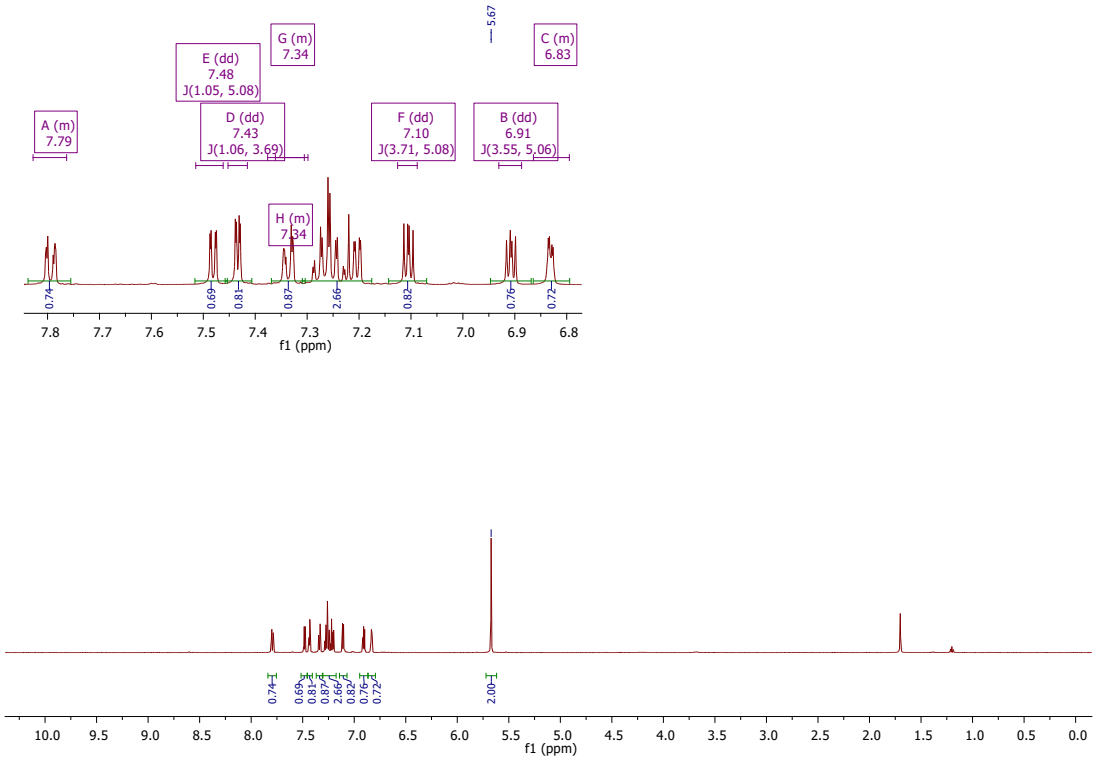

Figure S9. ^{1}H NMR spectra of **L^{5}** in $CDCl_3$.

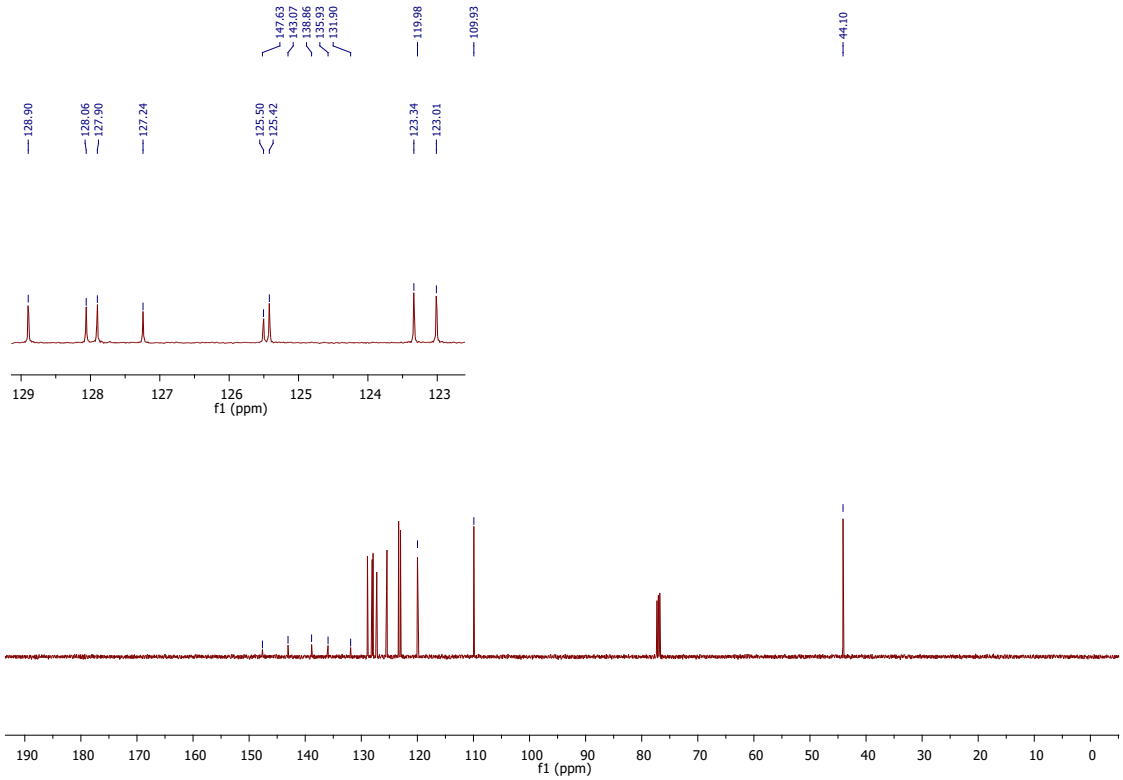

Figure S10. ^{13}C NMR spectra of **L^{5}** in $CDCl_3$.

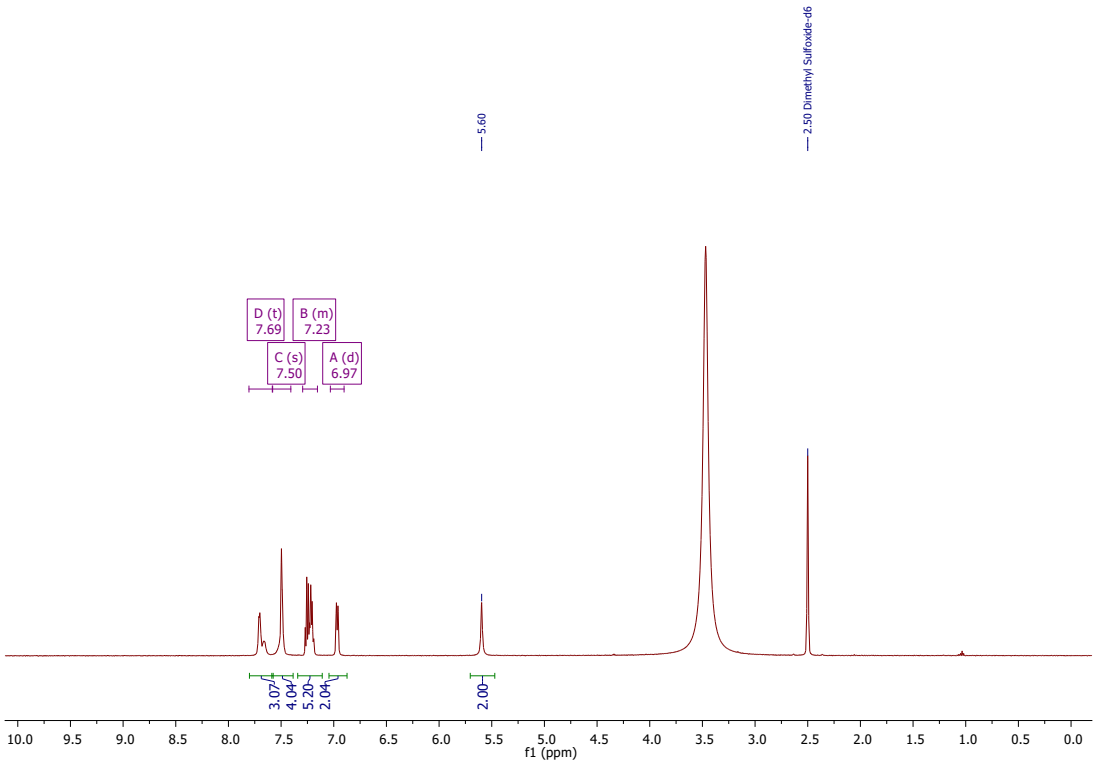

Figure S11. ^{1}H NMR spectra of **1** in DMSO-d^6.

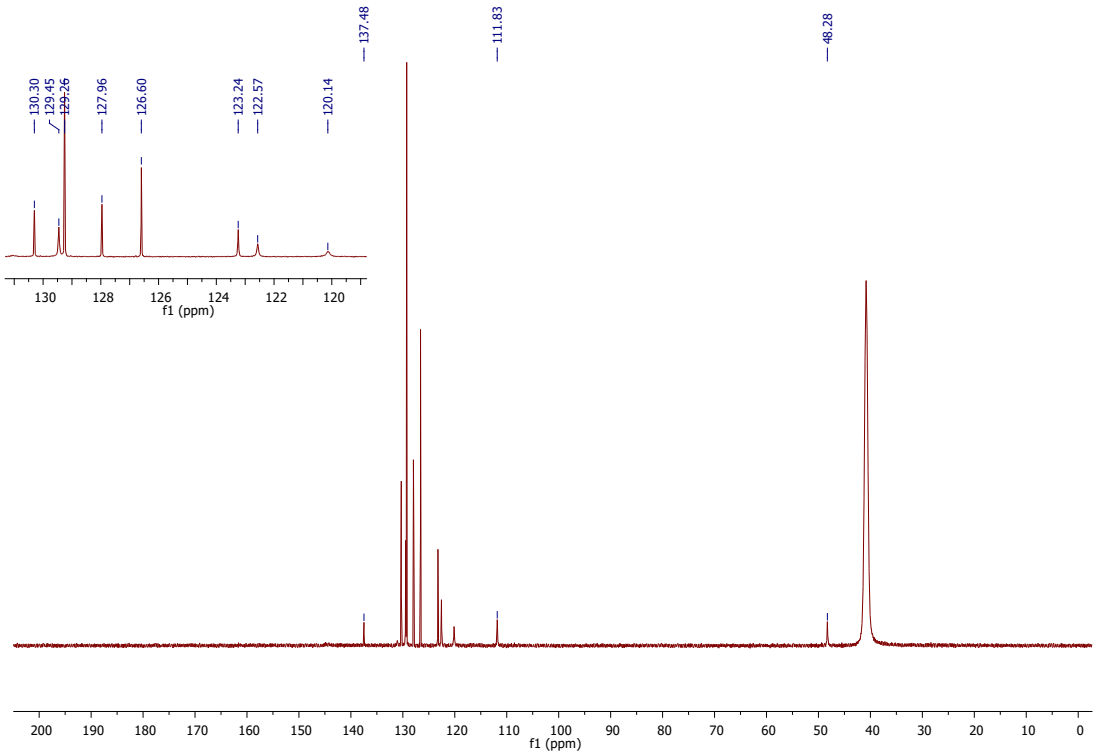

Figure S12. ^{13}C NMR spectra of **1** in DMSO-d^6.

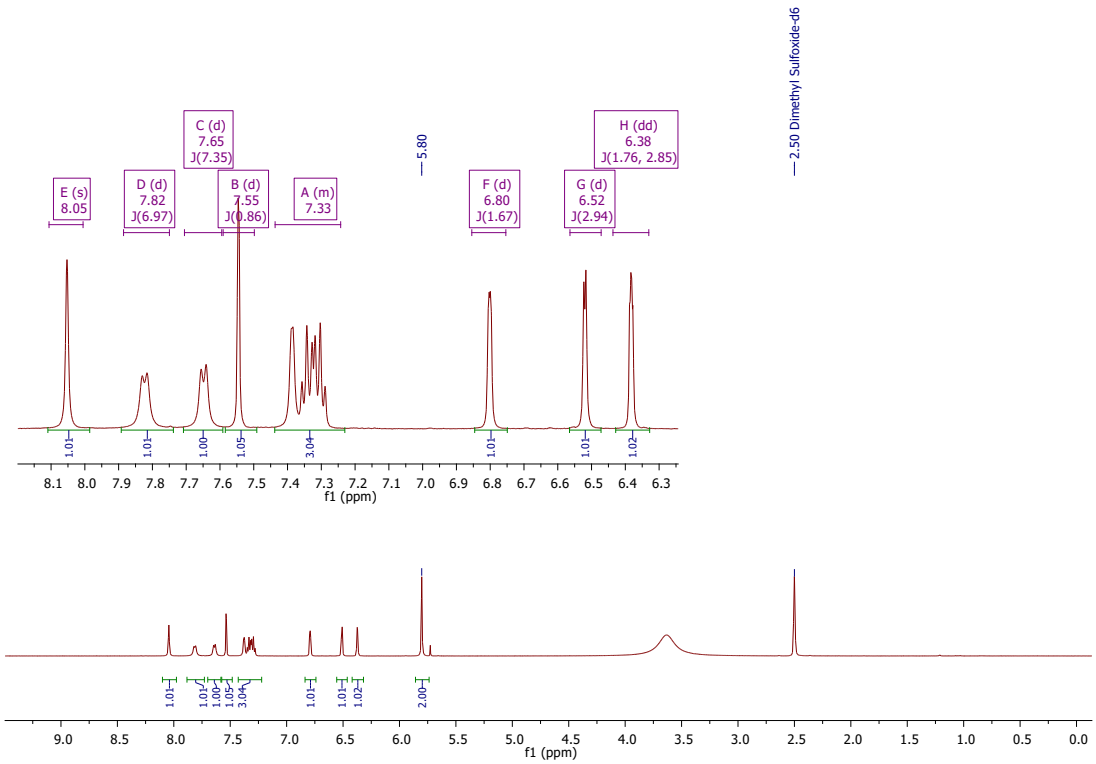

Figure S13. ^{1}H NMR spectra of **2** in DMSO-d^6.

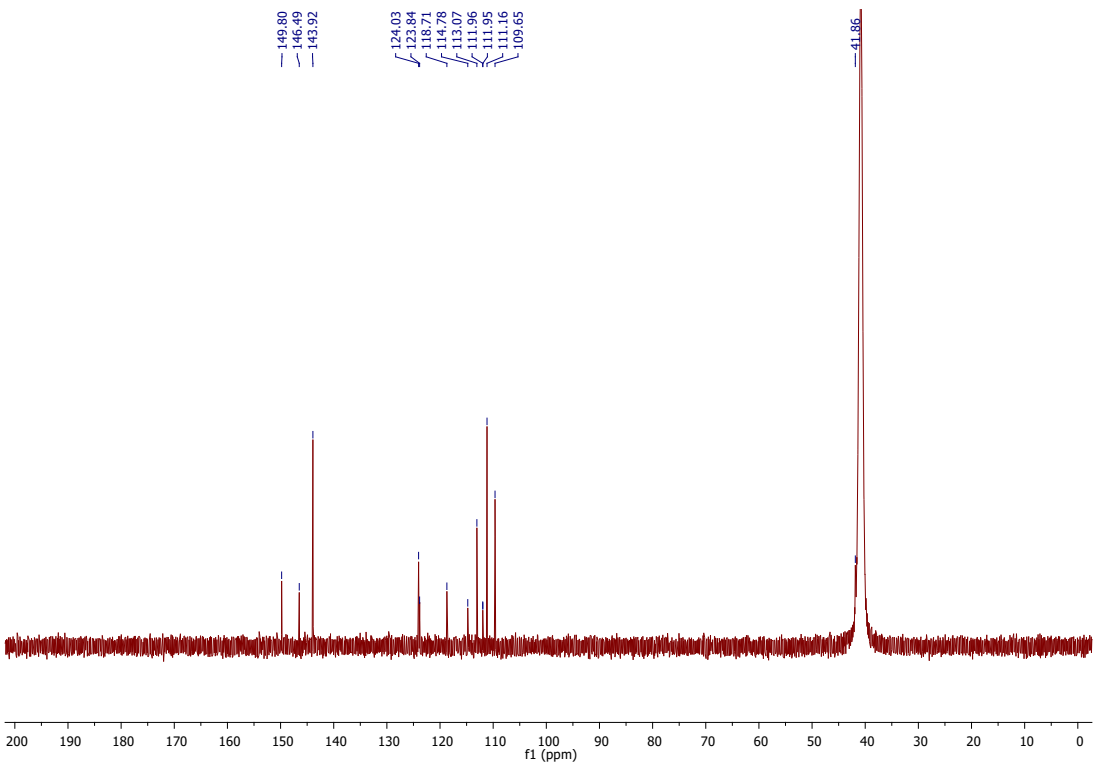

Figure S14. ^{13}C NMR spectra of **2** in DMSO-d^6.

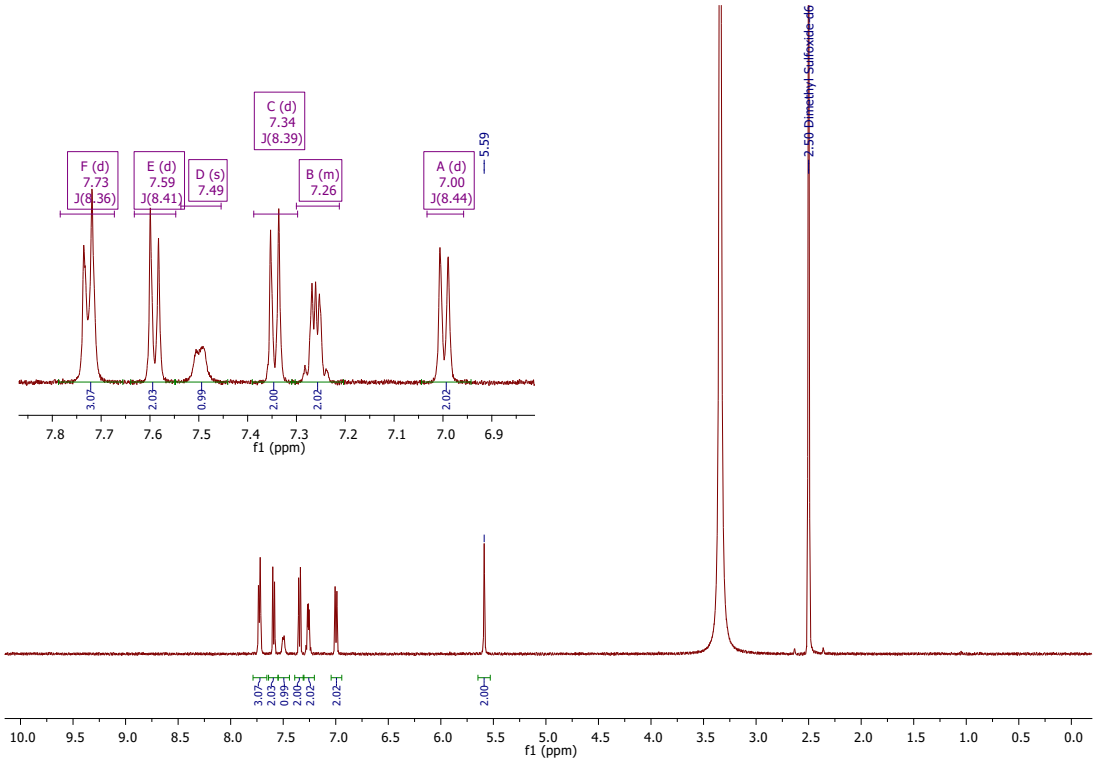

Figure S15. ^{1}H NMR spectra of **3** in DMSO-d^6.

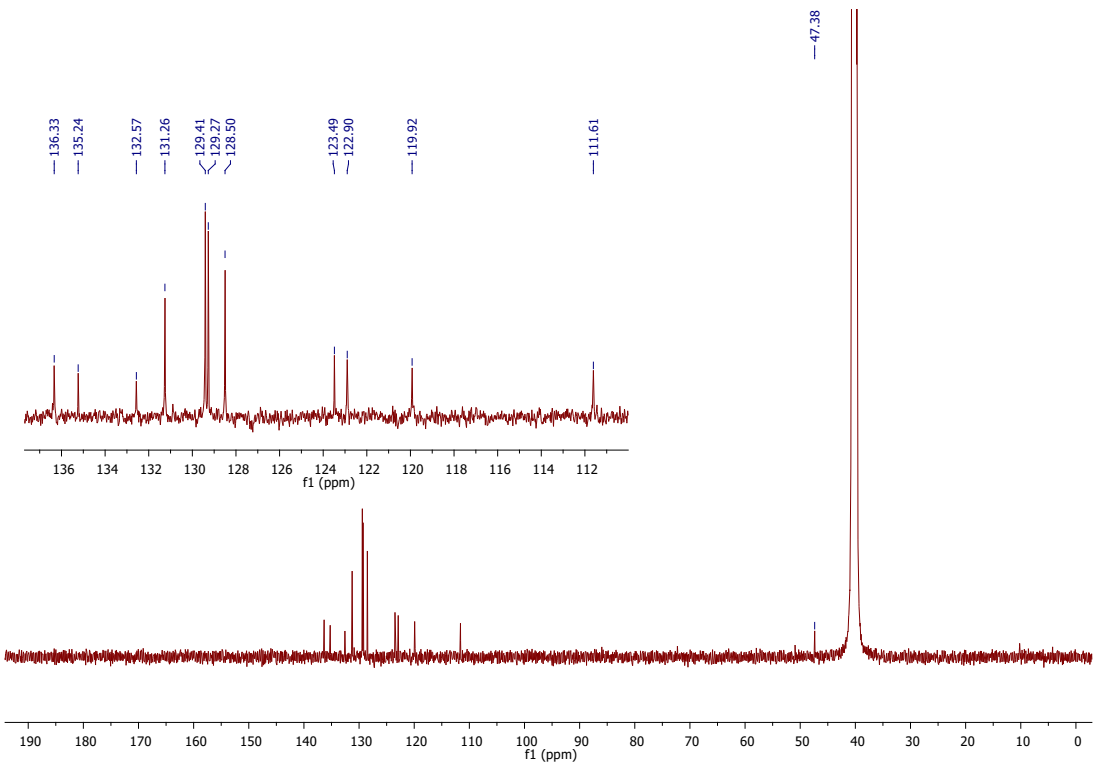

Figure S16. ^{13}C NMR spectra of **3** in DMSO-d^6.

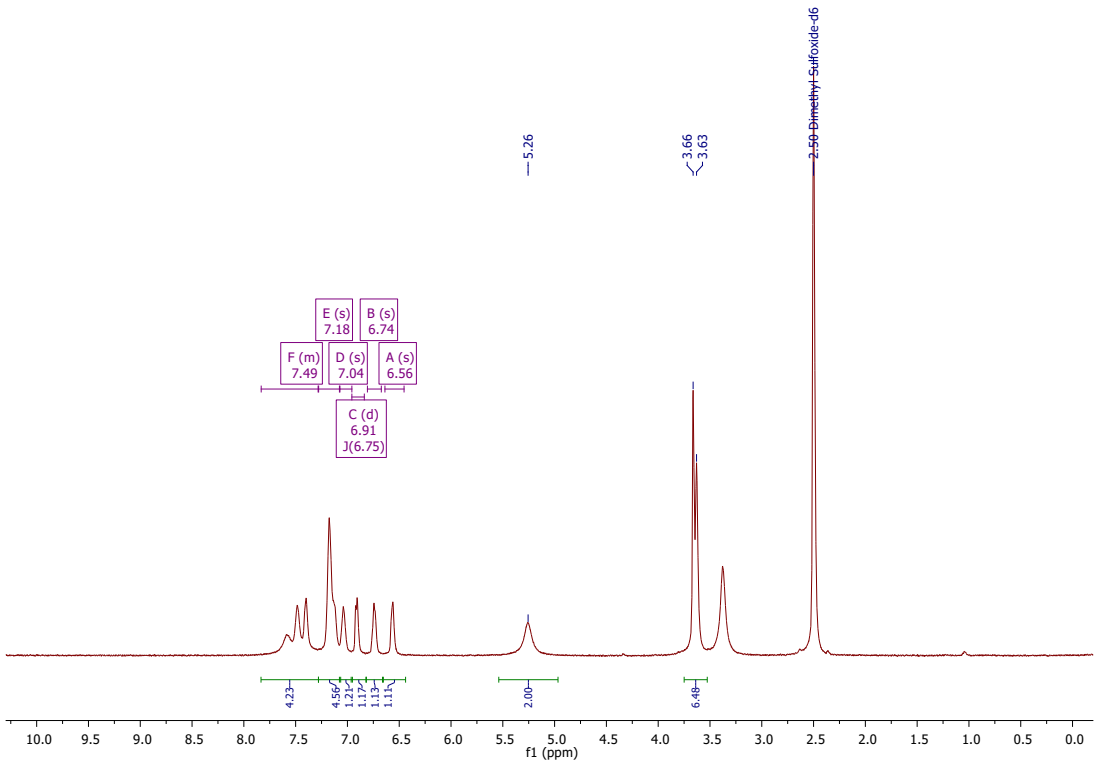

Figure S17. ^{1}H NMR spectra of **4** in DMSO-d^6.

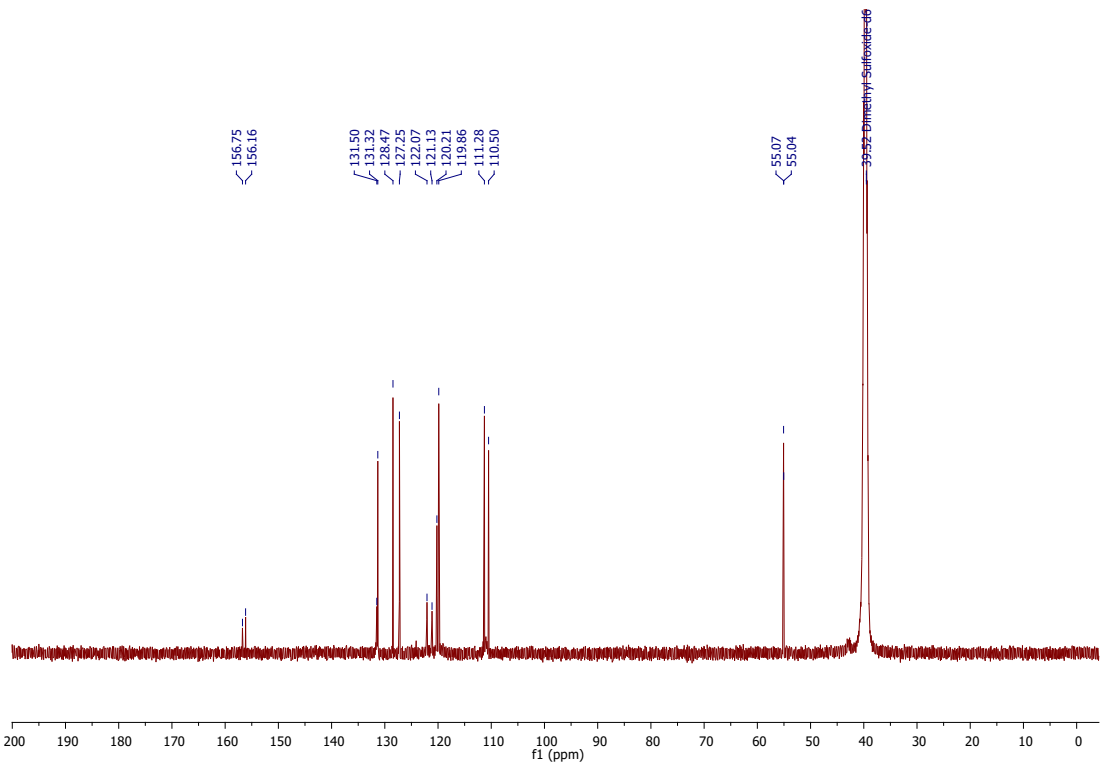

Figure S18. ^{13}C NMR spectra of **4** in DMSO-d^6.

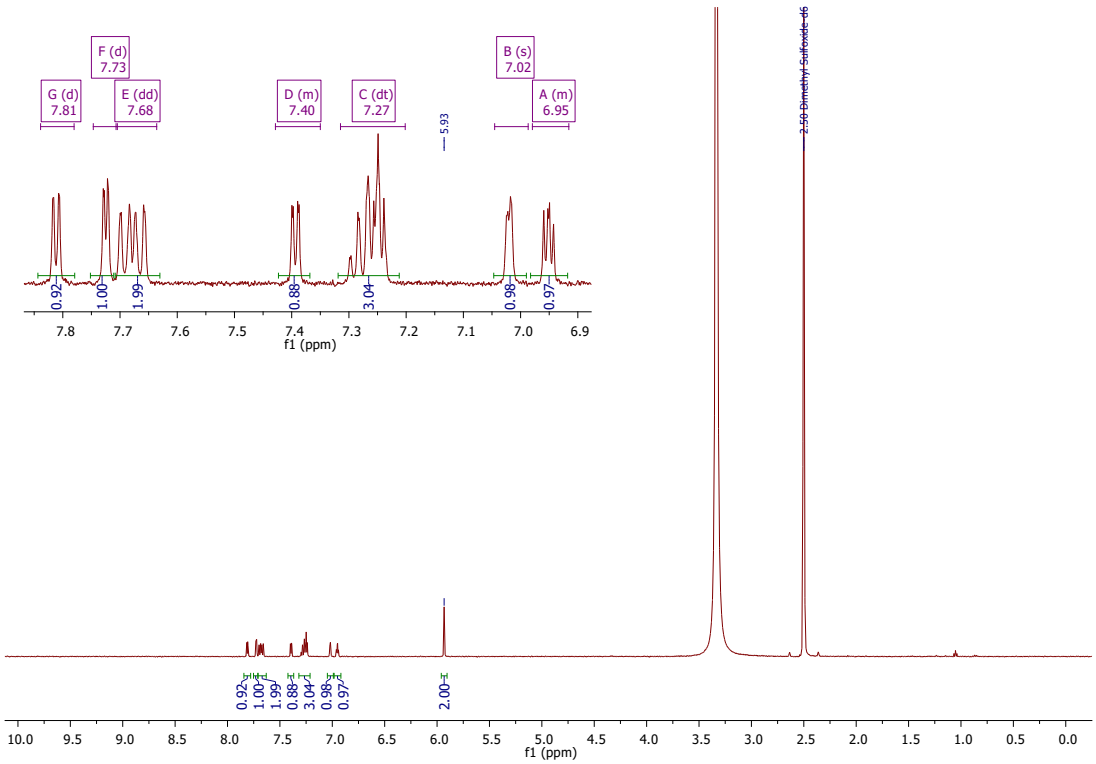

Figure S19. ^{1}H NMR spectra of **5** in DMSO-d^6.

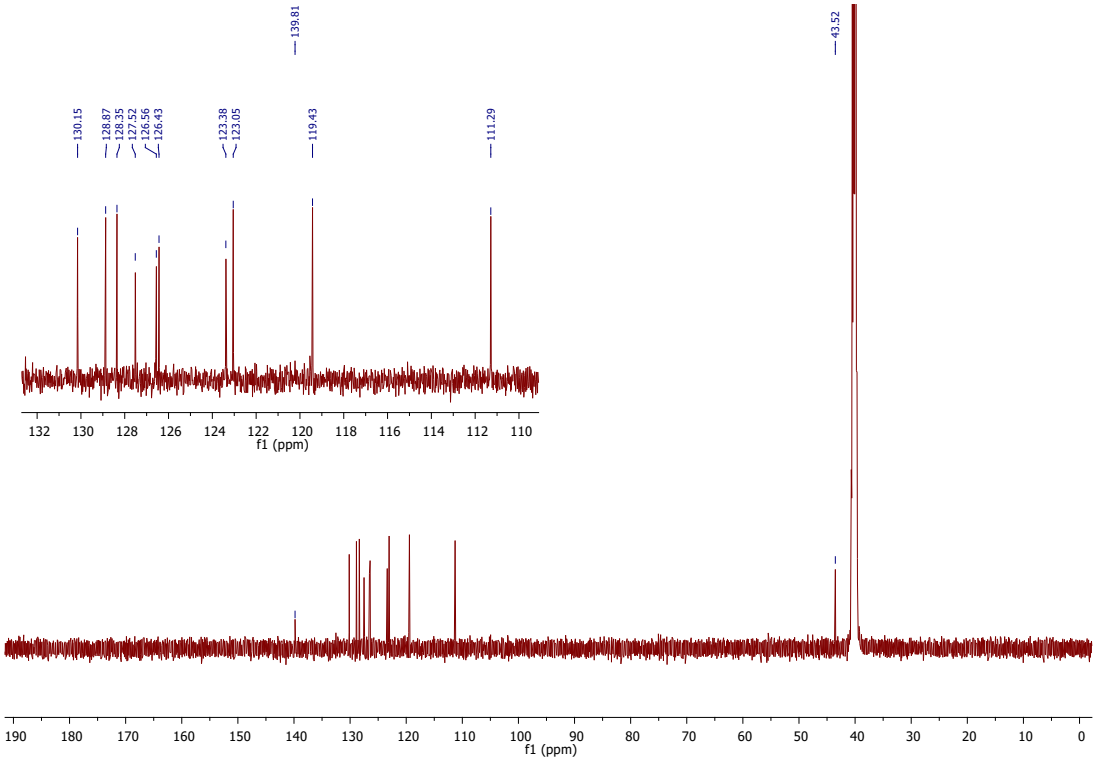

Figure S20. ^{13}C NMR spectra of **5** in DMSO-d^6.

1.2. Infrared spectroscopy

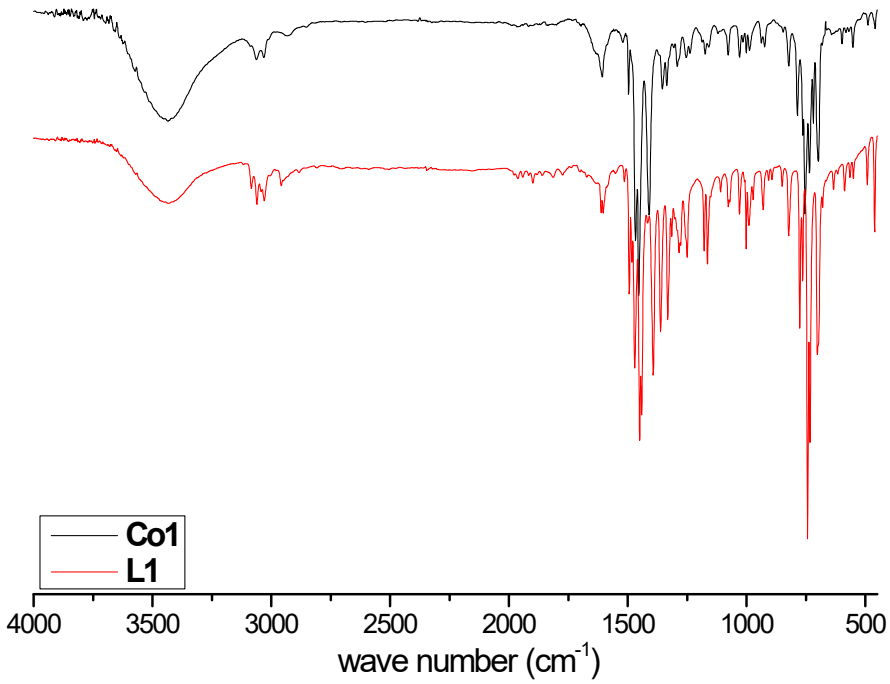

Figure S21. IR spectra of **L**[1] and **1**.

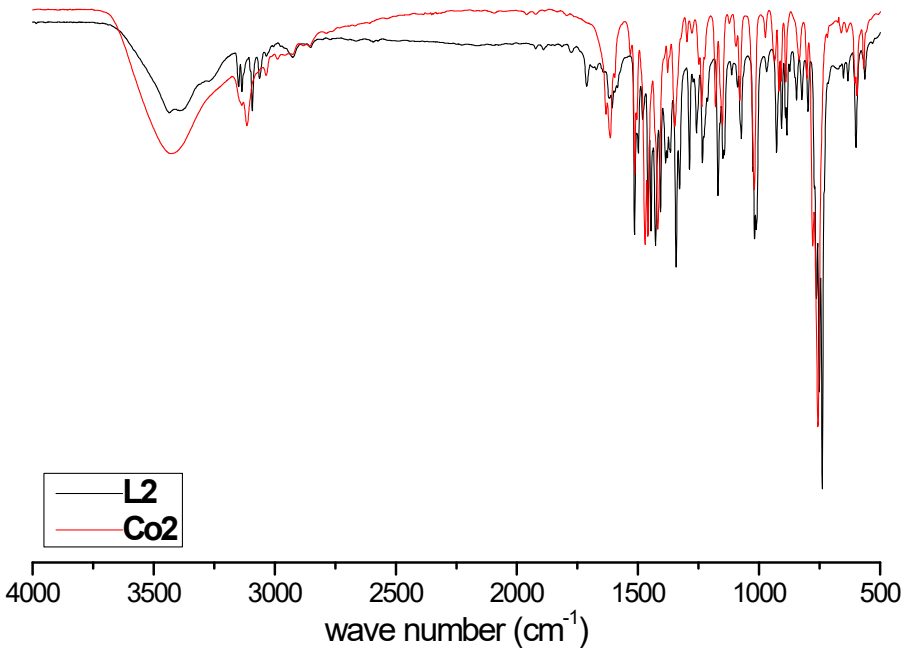

Figure S22. IR spectra of **L**[2] and **2**.

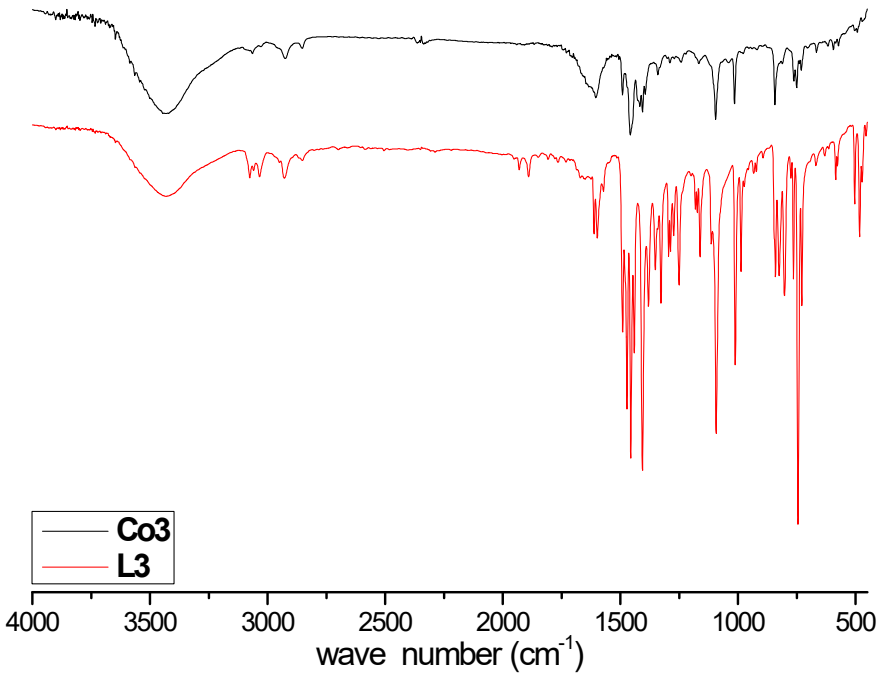

Figure S23. IR spectra of **L**^{3} and **3**.

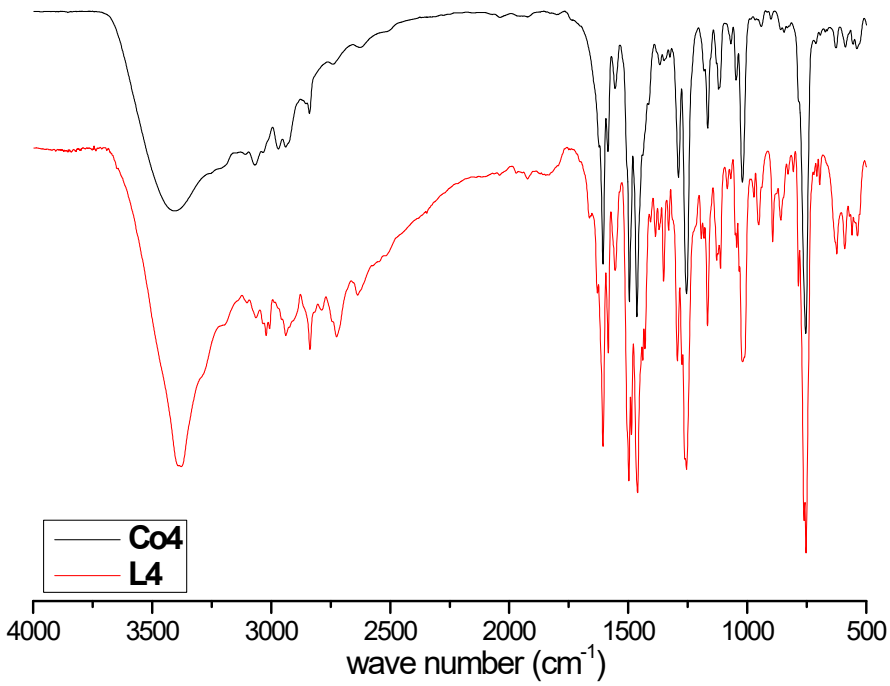

Figure S24. IR spectra of **L**^{4} and **4**.

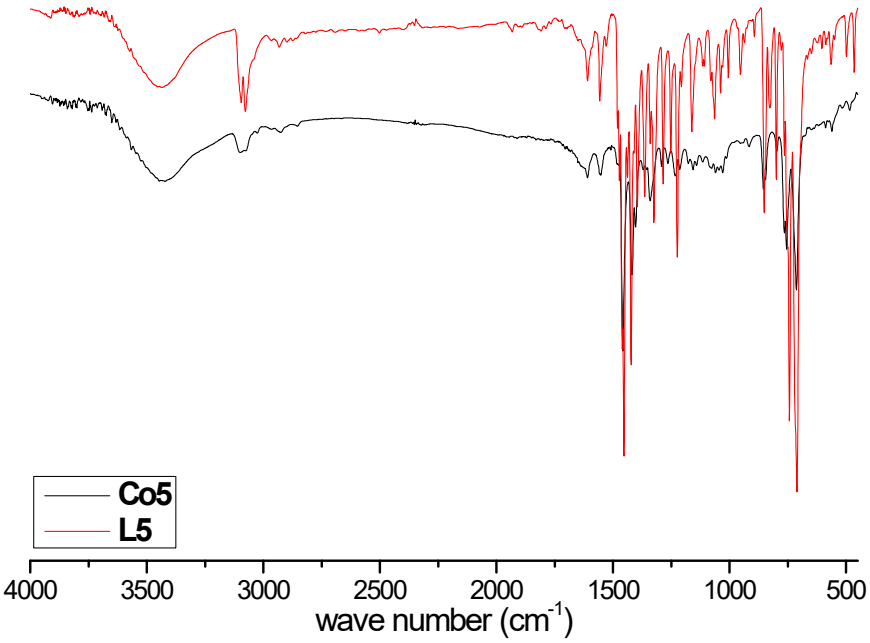

Figure S25. IR spectra of **L**^{5} and **5**.

1.3. ESI-HRMS

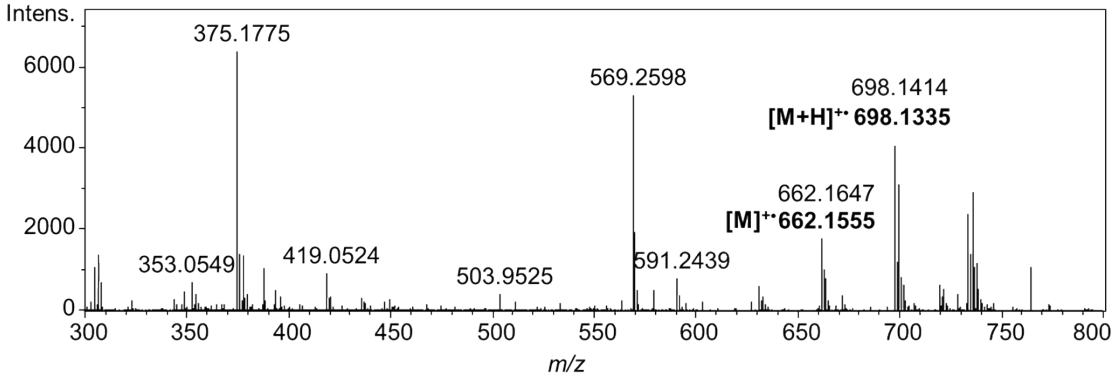

Figure S26. ESI-HRMS of **1**.

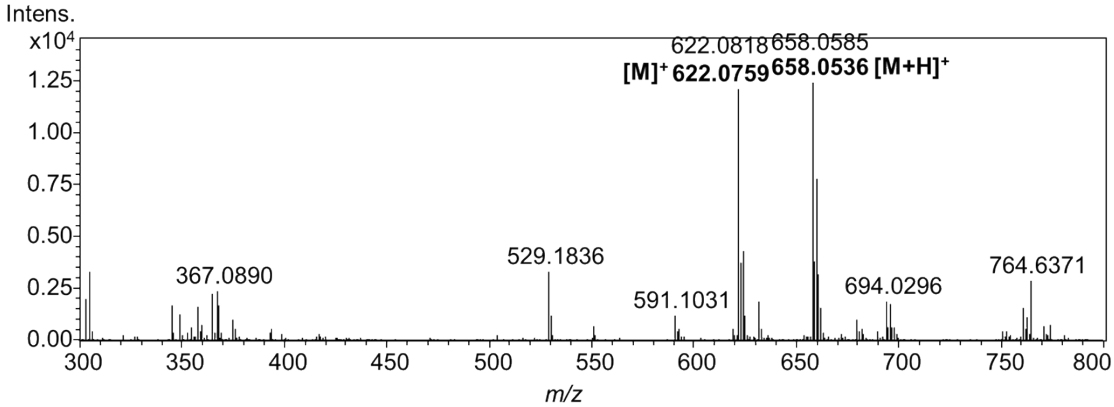

Figure S27. ESI-HRMS of **2**.

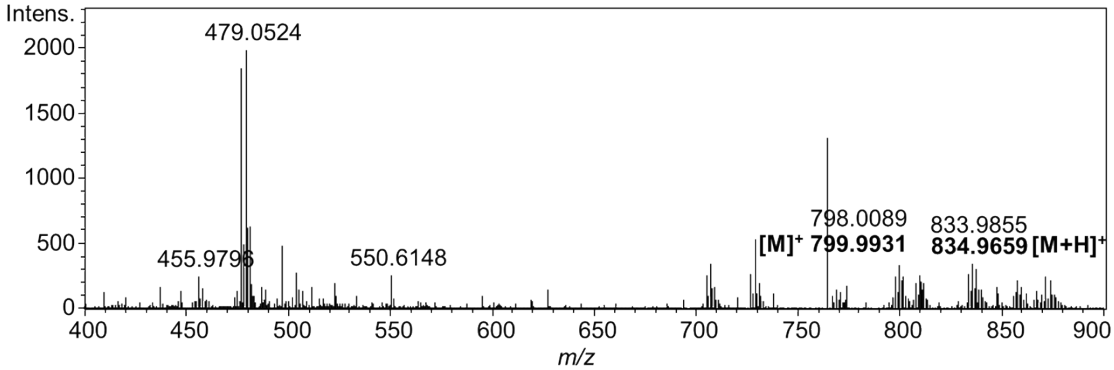

Figure S28. ESI-HRMS of **3**.

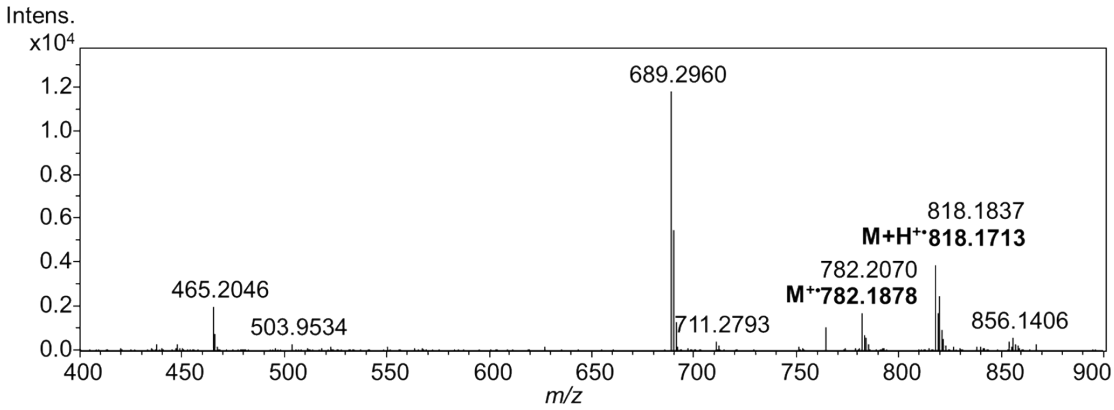

Figure S29. ESI-HRMS of **4**.

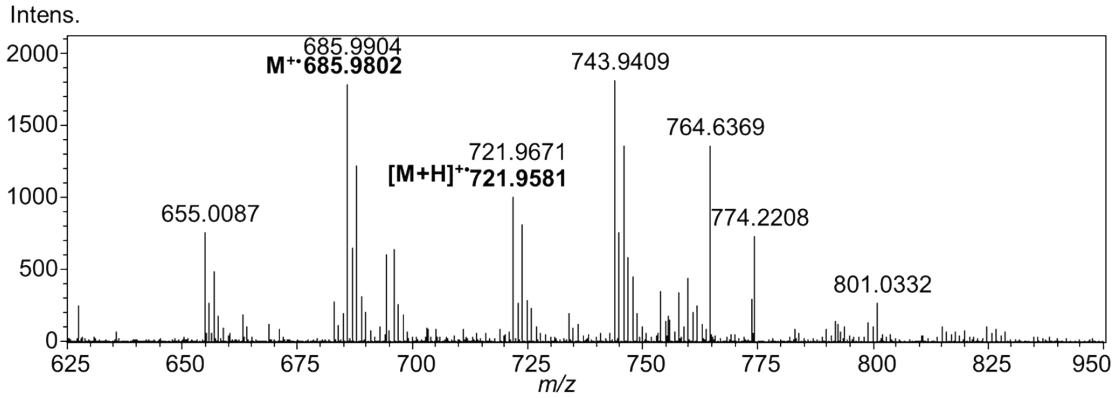

Figure S30. ESI-HRMS of **5**.

1.4. Electronic spectra

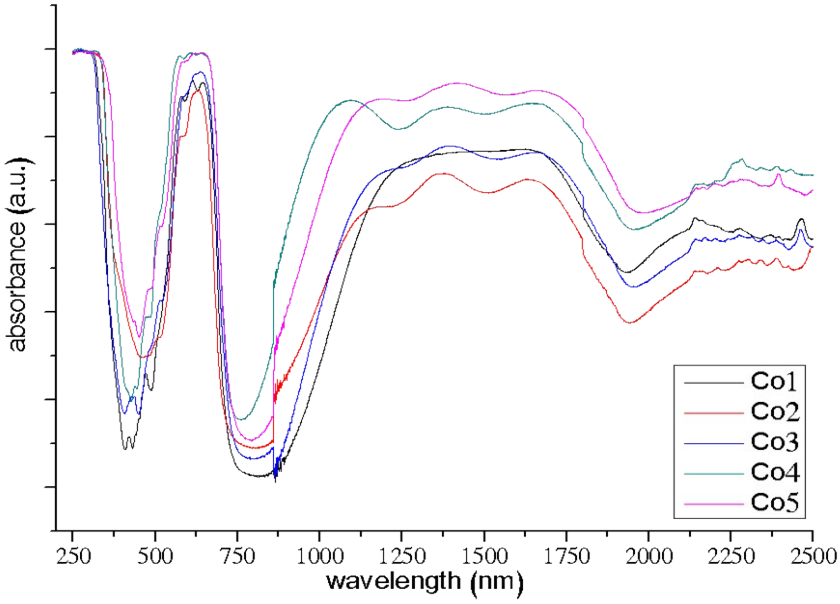

Figure S31. Electronic spectra of **1**–**5**.

Table S1. Observed and calculated values of electronic transitions and parameters for **1**–**5**

Compound	$\nu_1{}^a$ (cm^{-1})	$\nu_2{}^a$ (cm^{-1})	$\nu_3{}^a$ (cm^{-1})	B^b (cm^{-1})	β^c (cm^{-1})	$\beta°$ (%)^d	Δ_T (cm^{-1})
1	4110	6944	16622	748	0.773	29	4,110
2	4390	7551	16680	737	0.762	31	4,390
3	4260	7335	16356	727	0.751	33	4,260
4	4575	7863	16764	726	0.750	33	4,575
5	4310	7419	16439	727	0.751	33	4,310

[a]Values of [$^4A_2 \rightarrow {}^4T_2$] ($\nu_1$), [$^4A_2 \rightarrow {}^4T_1(F)$] ($\nu_2$) and [$^4A_2 \rightarrow {}^4T_1(P)$] ($\nu_3$). [b]Interelectronic Racah´s repulsion parameter; [c]Nephelauxetic ratio defined as the $B_{complex}/B'_{free\ ion}$ quotient with $B'_{free\ ion}$ = 967 cm^{-1}. [d]$\beta° = (B_{free\ ion} - B_{complex})/B_{free\ ion}$ x 100.

1.5. Thermogravimetric analysis

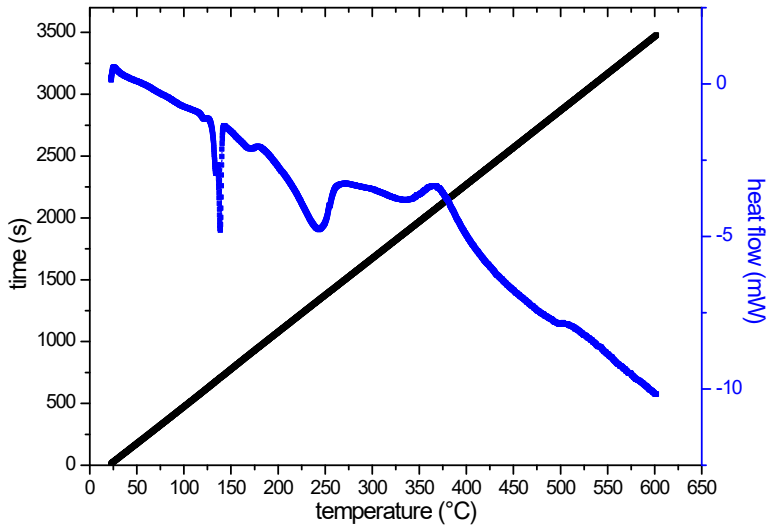

Figure S32. DSC curve of **L**[1].

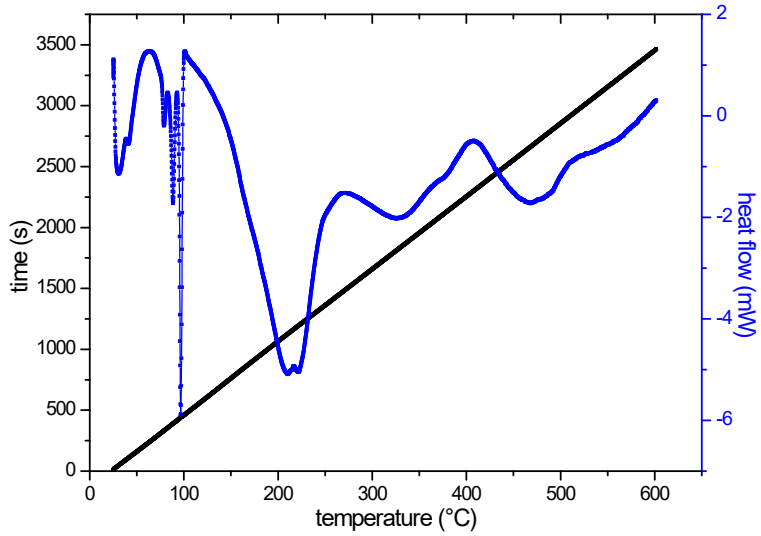

Figure S33. DSC curve of **L**[2].

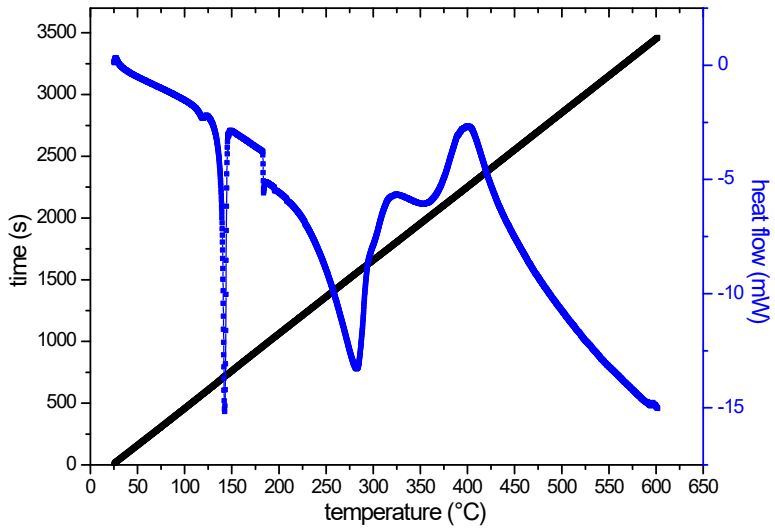

Figure S34. DSC curve of **L**[3].

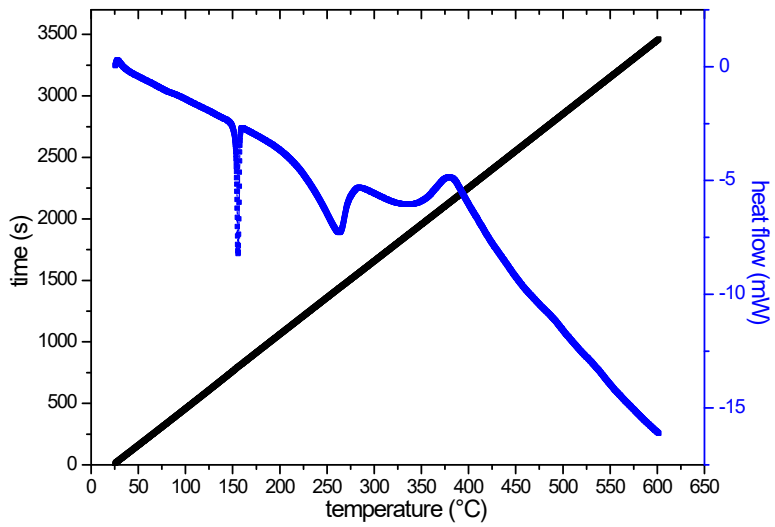

Figure S35. DSC curve of **L**[4].

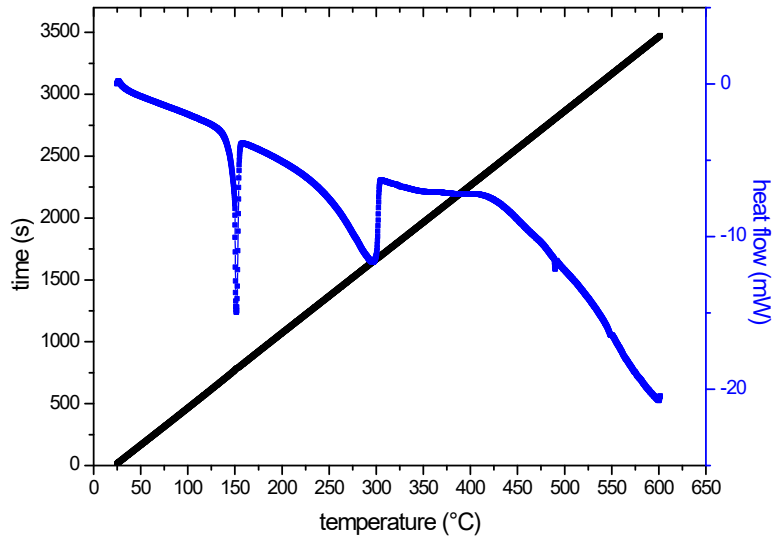

Figure S36. DSC curve of **L**[5].

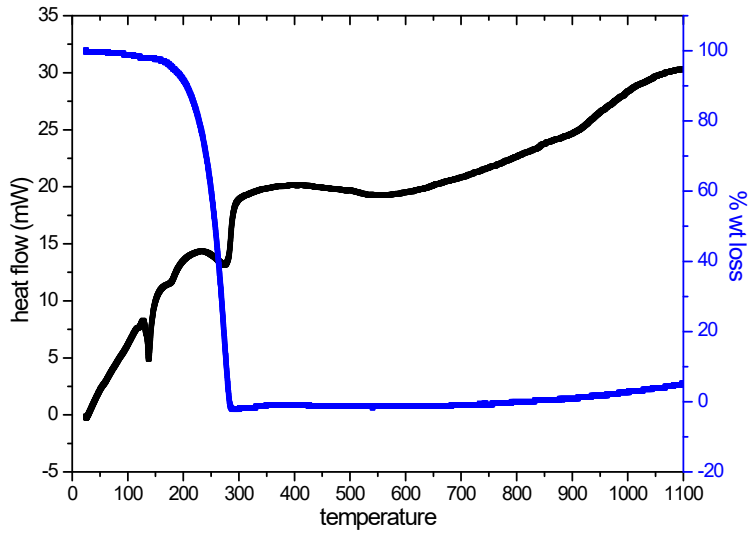

Figure S37. TG and DTG curves of **L**[1].

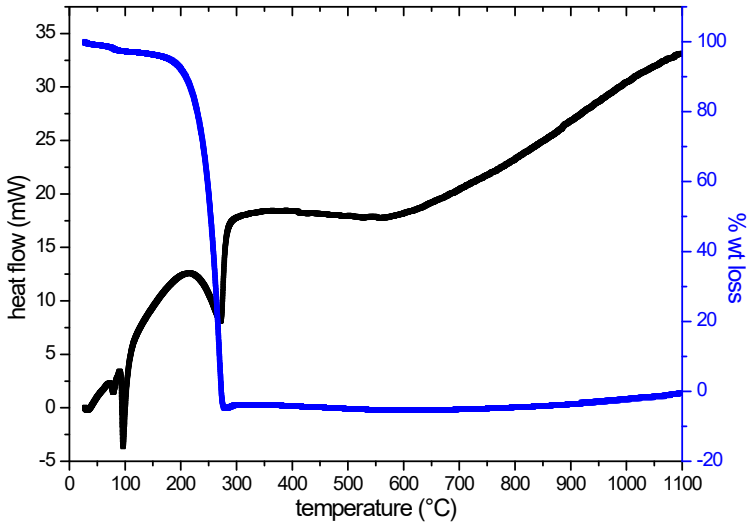

Figure S38. TG and DTG curves of **L²**.

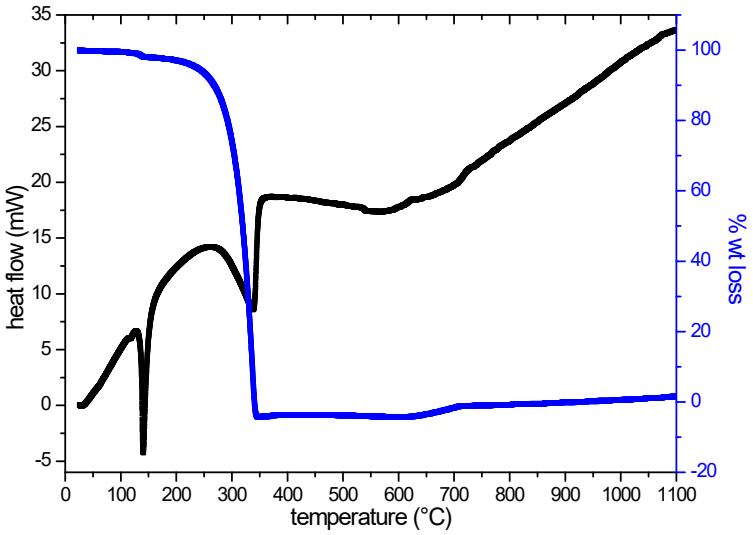

Figure S39. TG and DTG curves of **L³**.

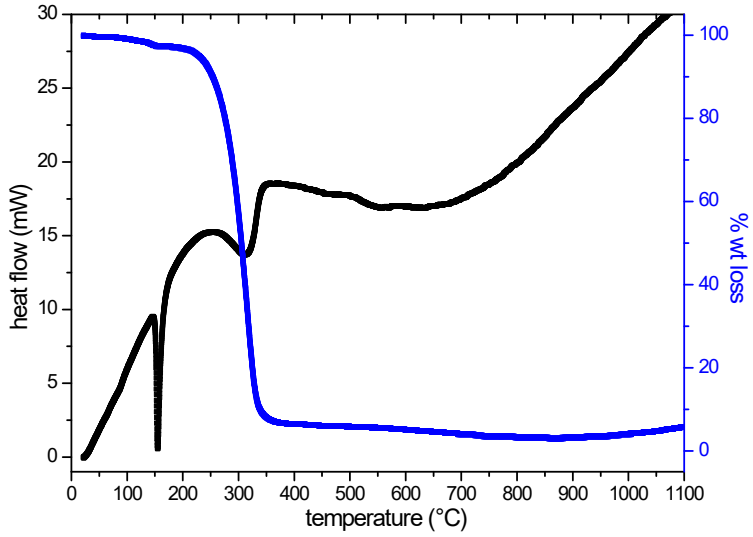

Figure S40. TG and DTG curves of **L⁴**.

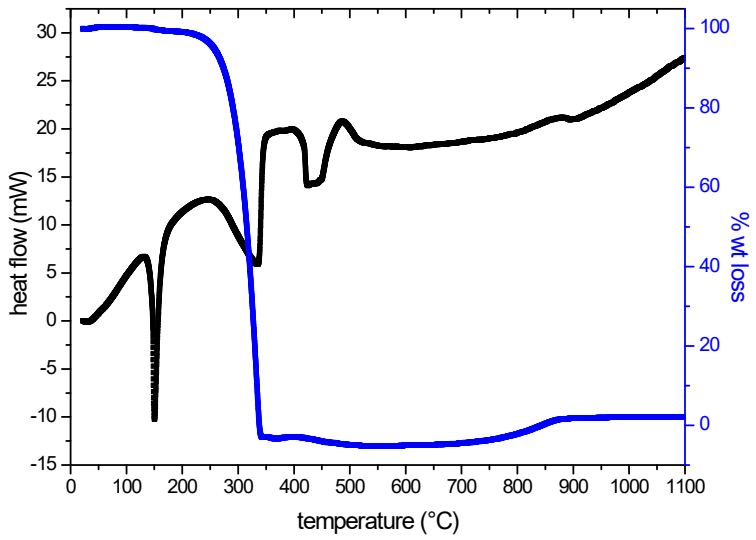

Figure S41. TG and DTG curves of **L**[5].

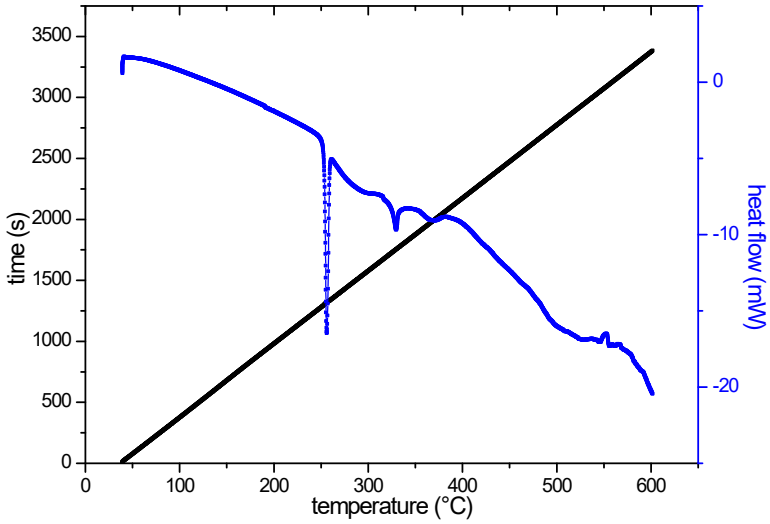

Figure S42. DSC curves of **Co1**.

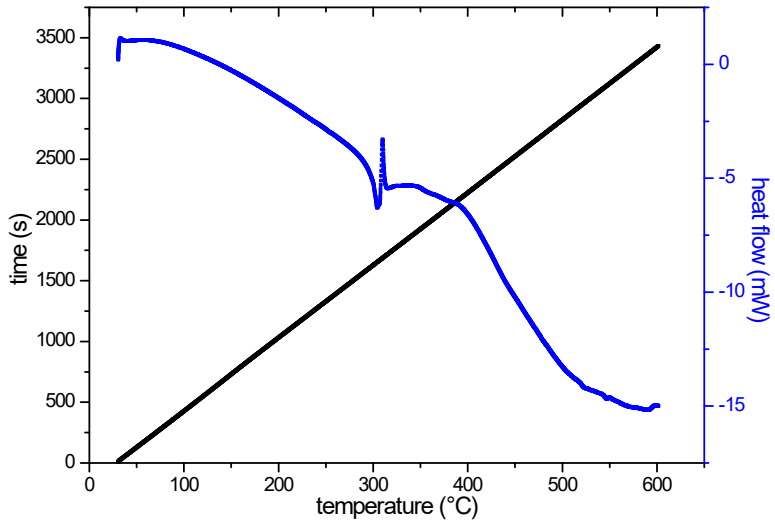

Figure S43. DSC curves of **Co2**.

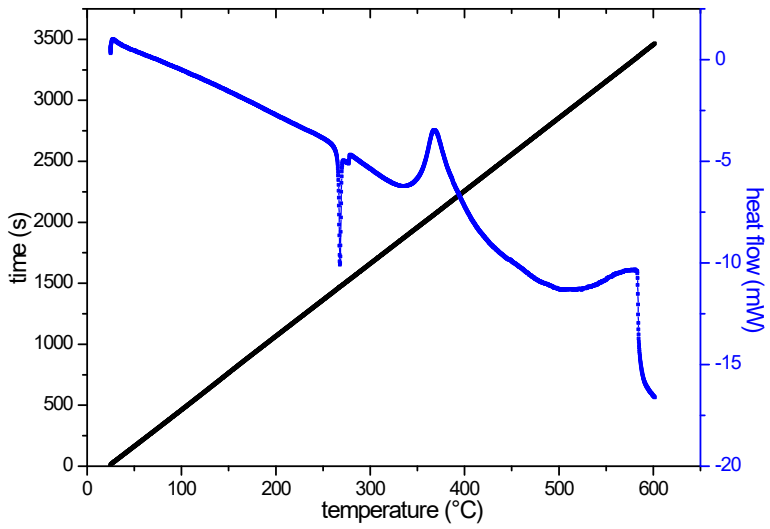

Figure S44. DSC curves of **Co3**.

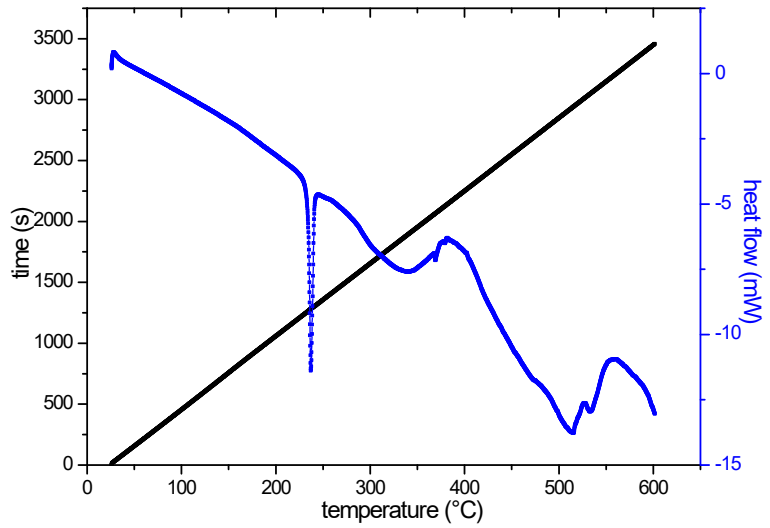

Figure S45. DSC curves of **Co4**.

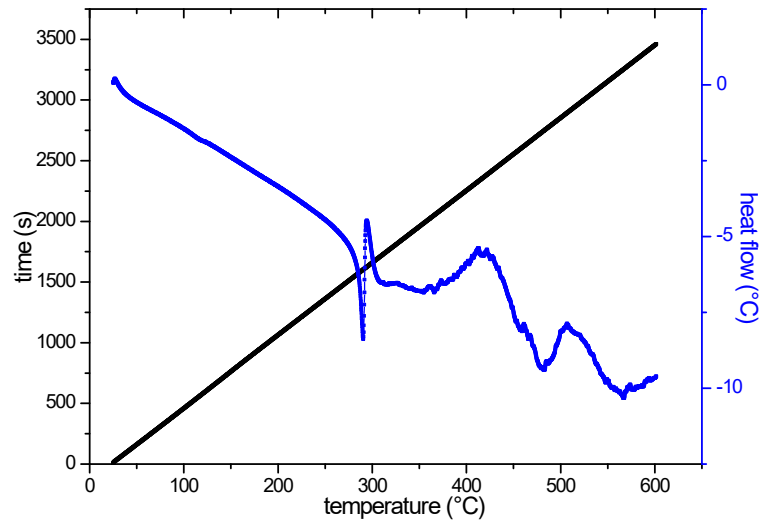

Figure S46. DSC curves of **Co5**.

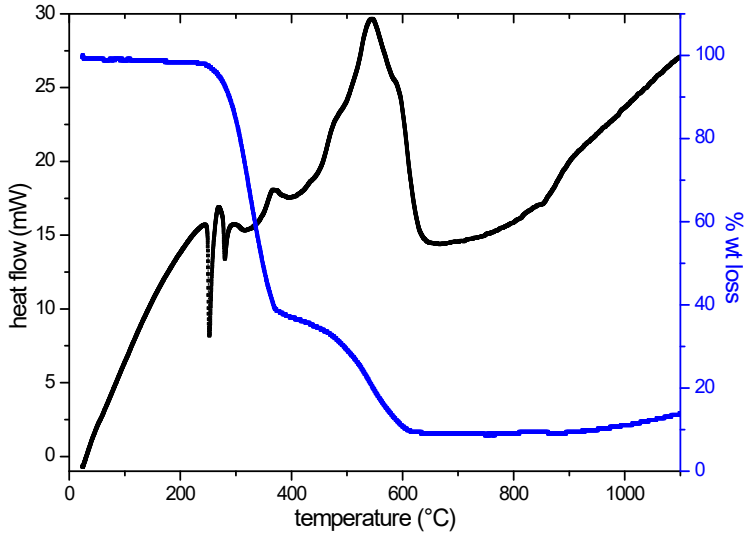

Figure S47. TG and DTG curves of **Co1**.

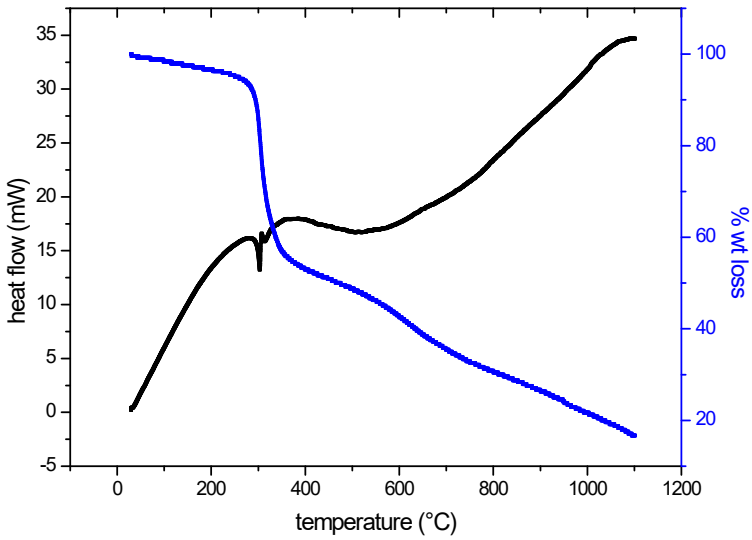

Figure S48. TG and DTG curves of **Co2**.

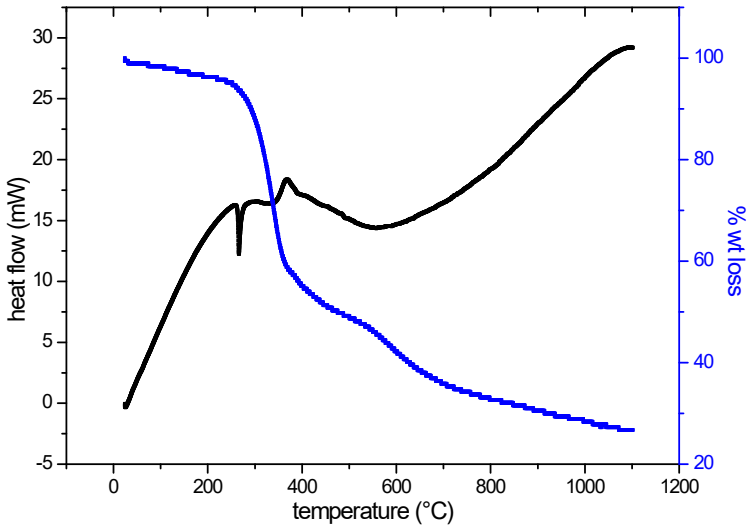

Figure S49. TG and DTG curves of **Co3.**

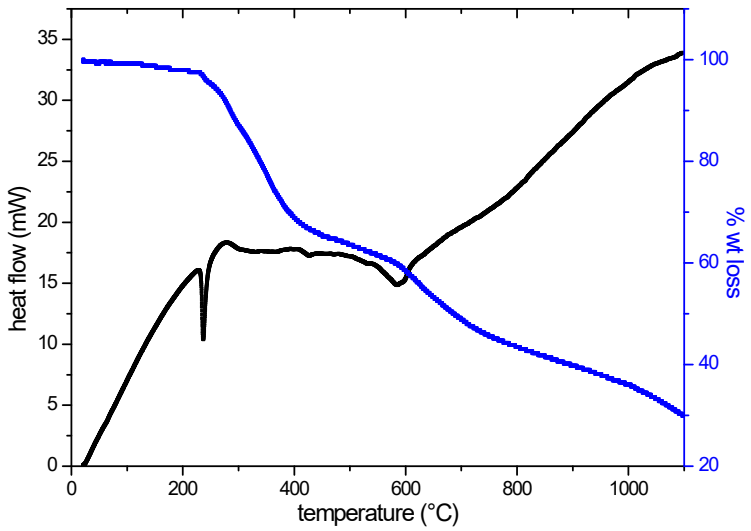

Figure S50. TG and DTG curves of **Co4**.

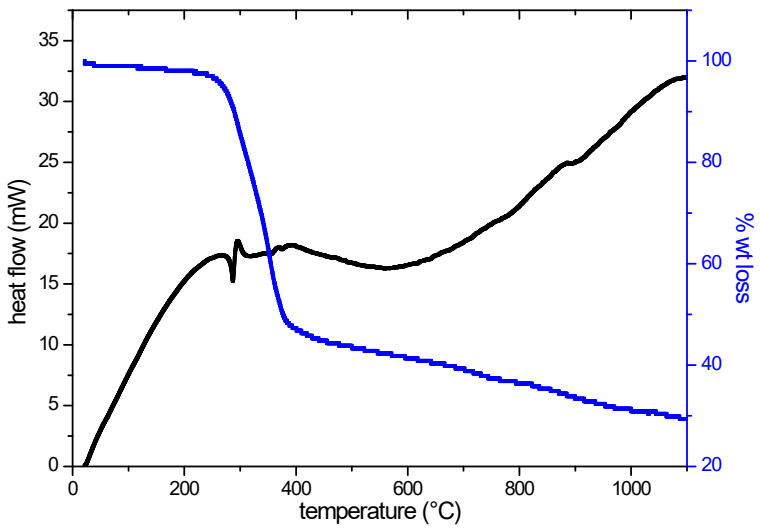

Figure S51. TG and DTG curves of **Co5**.

1.6. X-ray crystallographic data collection and crystal structure

Table S2. Crystal data and refinement statistics for the structures of **1**, **3**, **4** and **5**.

		1	**3**	**4**	**5**
Chemical formula		$[CoCl_2(L_1)_2]$	$[CoCl_2(L_3)_2]$	$[CoCl_2(L_4)_2]$	$[CoCl_2(L_5)_2]$
Fw (g mol^{-1})		698.53	836.29	818.63	722.62
Cryst system		Triclinic	Orthorhombic	Monoclinic	Monoclinic
Space group		*P*-1	*Pbca*	*C*2/*c*	*C*2/*c*
Z		2	8	8	4
T (K)		296(2)	296(2)	296(2)	296(2)
Unit cell dimensions	*a*	10.1122(2)	18.8282(8)	46.6731(11)	15.6162(10)
	b	11.0132(2)	9.5569(4)	11.7655(3)	11.2424(7)
	c	16.9563(4)	42.2102(13)	14.8882(4)	19.1016(16)
	α	81.2620(10)	90	90	90
	β	79.356(2)	90	100.070(2)	112.182(2)
	γ	65.0490(10)	90	90	90
V (Å^3)		1676.87(6)	7595.3(5)	8049.6(4)	3105.3(4)
ρ_{calc} (Mg/m^3)		1.383	1.463	1.351	1.546
Absorption coefficient μ (mm^{-1})		5.747	7.704	4.946	1.025
*Θ r*ange for data collection (°)		4.988-66.590	2.093-66.607	1.923-66.409	2.303-25.408
Index ranges	*h*	-12 to 11	-21 to 22	-54 to 54	-17 to 18
	k	-12 to 13	-11 to 5	-13 to 7	-13 to 10
	l	-13 to 20	-48 to 49	-17 to 17	-23 to 23
Observed reflections		5778	6579	6970	2859
[$I > 2\sigma(I)$]					
Unique reflections		4344	3692	3179	2383
Symmetry factor (R_{int})		0.0421	0.1354	0.1483	0.0418
Completeness to θ_{max} (%)		97.6	98.0	98.6	99.7
F(000)		722	3400	3400	1476
Refined parameters		424	460	497	231

Goodness-of-fit on F^2 (S)[a]	1.023	1.108	1.029	1.069
Final R_1[b] factor [I > 2σ(I)]	0.0421	0.0620	0.0986	0.0876
wR_2[c] factor (all data)	0.1103	0.1721	0.3267	0.3057
Largest diff. peak/hole (e Å^{-3})	0.244/-0.263	0.682/-0.352	0.959/-0.479	0.984/-0.964
CCDC deposit no.	1822401	1822403	1822402	1822400

$$^{a}S = \left[\frac{\sum w_{hkl}(F^2_{(hkl)\mathrm{obs}} - F^2_{(hkl)\mathrm{calc}})^2}{|N_r - N_p|}\right]^{1/2}, \; ^{b}R = \frac{\sum \left| |F_{(hkl)\mathrm{obs}}| - |F_{(hkl)\mathrm{calc}}| \right|}{\sum |F_{(hkl)\mathrm{obs}}|}, \; ^{c}wR_2 = \left[\frac{\sum w_{hkl}(F^2_{(hkl)\mathrm{obs}} - F^2_{(hkl)\mathrm{calc}})^2}{\sum w_{hkl} F^2_{(hkl)\mathrm{obs}}}\right]^{1/2}.$$

Table S3. Selected bond lengths (Å) and angles (°) for compounds **1**, **3**, **4** and **5**[a,b]

	1	**3**	**4**	**5**
Co1-N1A	2.041(2)	2.037(4)	2.056(6)	2.024(4)
Co1-N1B	2.053(2)	2.052(4)	2.005(7)	2.024(4)
Co1-Cl1	2.2600(9)	2.2331(15)	2.252(3)	2.2552(15)
Co1-Cl2	2.2601(9)	2.2584(15)	2.237(3)	2.2552(15)
N1A-Co1-N1B (α)	121.20(9)	113.92(16)	110.0(3)	109.8(2)
Cl1-Co1-Cl2 (β)	111.95(4)	108.09(7)	119.12(10)	109.99(12)
N1A-Co1-Cl1 (τ_1)	97.74(7)	110.64(12)	98.18(18)	106.21(11)
N1B-Co1-Cl2 (τ_1')	98.67(7)	114.20(12)	102.9(2)	106.21(11)
N1A-Co1-Cl2 (τ_2)	114.80(7)	105.49(12)	107.67(19)	112.34(11)
N1B-Co1-Cl1 (τ_2')	113.16(7)	104.45(11)	118.4(2)	112.34(11)

[a] In the structure of **4**, N1A = N1, N1B = N1^{i} and Cl2 = Cl1^{i} [Symmetry code: (i) = 2–x, y, 1/2–z]. [b]The meaning of the α, β, τ_1, τ_1', τ_2, and τ_2' parameters is illustrated in Figure 2 (see below).

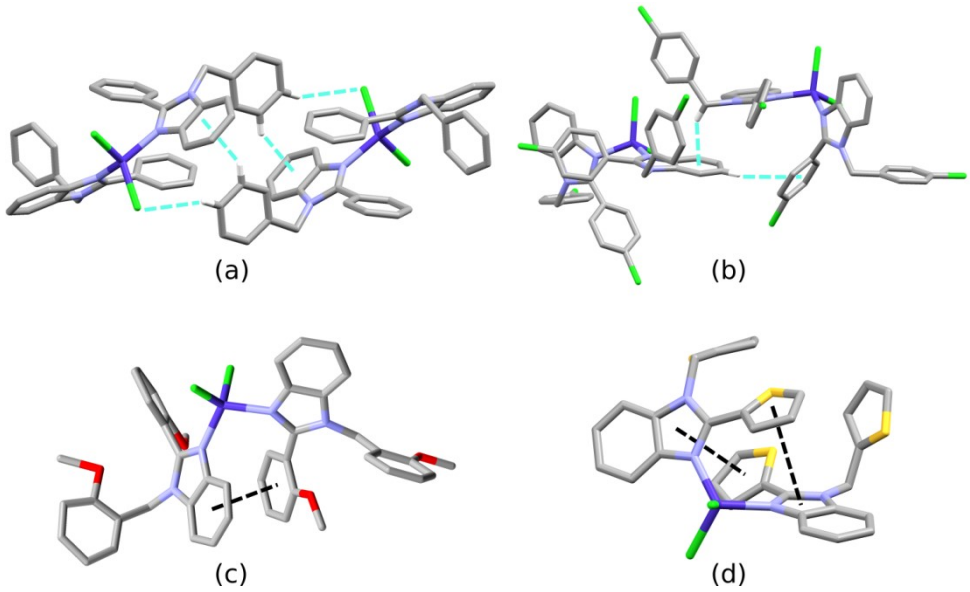

Figure S52. Intermolecular and intramolecular interactions driving drove a so-called locked geometry in coordination compounds found in **1** (a), **3** (b), **4** (c) and **5** (d). Dashed cyan lines indicates C-H···π and C-H···Cl type interactions, while dashed black lines represent the π···π contacts.

1.7. EPR spectra and theoretical calculations

Table S4. Theoretical magnetic parameters evaluated for **1**–**5**

Compound	Effective SOC Hamiltonian[a]			2nd order perturbative SOC[a]	
	g_x, g_y, g_z	D (cm^{-1})	E/D	D (cm^{-1})	E/D
1	2.254, 2.258, 2.338	–6.81	0.012	–6.82	0.024
2	2.252, 2.265, 2.293	–2.63	0.197	+3.29	0.298
3	2.264, 2.280, 2.284	+1.86	0.043	+2.60	0.066
4	2.216, 2.286, 2.314	+9.98	0.200	+9.62	0.198
5	2.266, 2.274, 2.284	–2.03	0.277	+2.79	0.286

[a]Values obtained by means of CAS/NEVPT2 calculations.

Table S5. Theoretical components of the *g*-factor evaluated for ground and excited Kramers doublet of **1**–**5**

Compound	Ground Kramers doublet[a]			Excited Kramers doublet[a]		
	g_1	g_2	g_3	g_1	g_2	g_3
1	0.072	0.084	7.016	2.351	4.435	4.590
2	1.138	1.387	6.636	2.059	3.139	5.655
3	2.249	4.271	4.855	0.284	0.298	6.791
4	1.974	3.185	5.799	1.166	1.398	6.424
5	1.456	1.877	6.426	1.853	2.663	5.997

[a]Values obtained by means of CAS/NEVPT2 calculations.

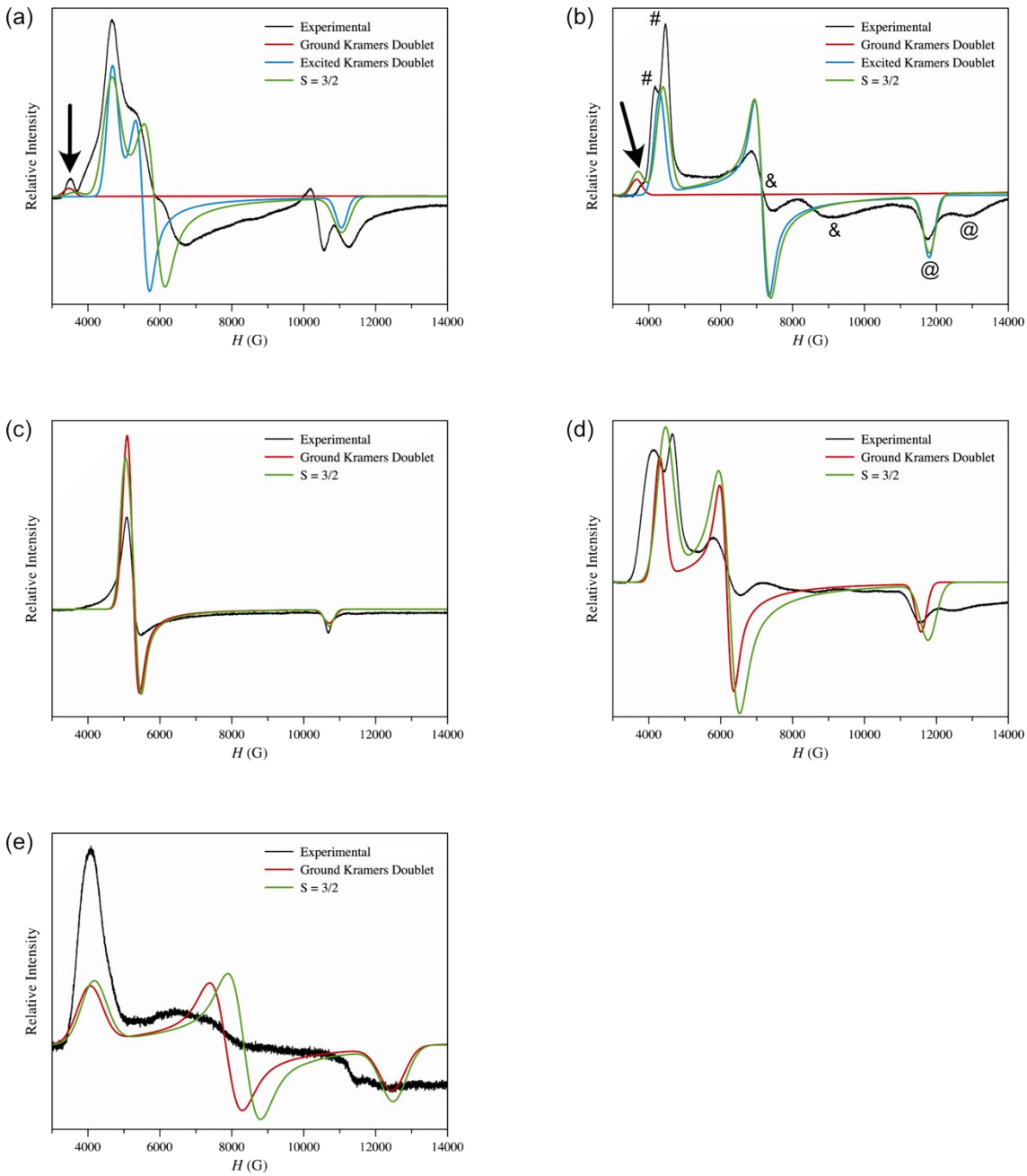

Figure S53. Experimental Q-band EPR spectra for **1-5** form (a) to (c) and their simulations from a zfs model applied on a S = 3/2 state or the ground (GKD) and excited (EKD) Kramers doublet through an effective spin (S_{eff} = ½) model. The simulations were done using the next values: (a) zfs: g_x = 2.354, g_y = 2.358, g_z = 2.358, D = –6.66 cm^{-1}, and E/D = 0.077; GKD: g_1 = 1.00, g_2 = 1.00, and g_3 = 7.00; EKD: g_1 = 2.20, g_2 = 4.40, and g_3 = 5.20; (b) zfs: g_x = 2.246, g_y = 2.274, g_z = 2.290, D = –3.09 cm^{-1}, and E/D = 0.159; GKD: g_1 = 1.14, g_2 = 1.39, and g_3 = 6.64; EKD: g_1 = 2.06, g_2 = 3.40, and g_3 = 5.65; (c) zfs: g_x = 2.364, g_y = 2.380, g_z = 2.271, D = +2.86 cm^{-1}, and E/D = 0.018; GKD: g_1 = 2.27, g_2 = 4.70, and g_3 = 4.70; (d) zfs: g_x = 2.316, g_y = 2.386, g_z = 2.131, D = +9.47 cm^{-1}, and E/D = 0.102; GKD: g_1 = 2.10, g_2 = 3.94, and g_3 = 5.65; (e) zfs: g_x = 2.284, g_y = 2.274, g_z = 2.266, D = +4.81 cm^{-1}, and E/D = 0.230; GKD: g_1 = 1.95, g_2 = 3.10, and g_3 = 6.00. The arrows point out the presence of a weak high magnetic field signal corresponding to the m_S = ±1/2 Kramers doublet. This notation, valid only for a null value of the E/D ratio, is used only to make easier the discussion.

1.8. Magnetic measurements

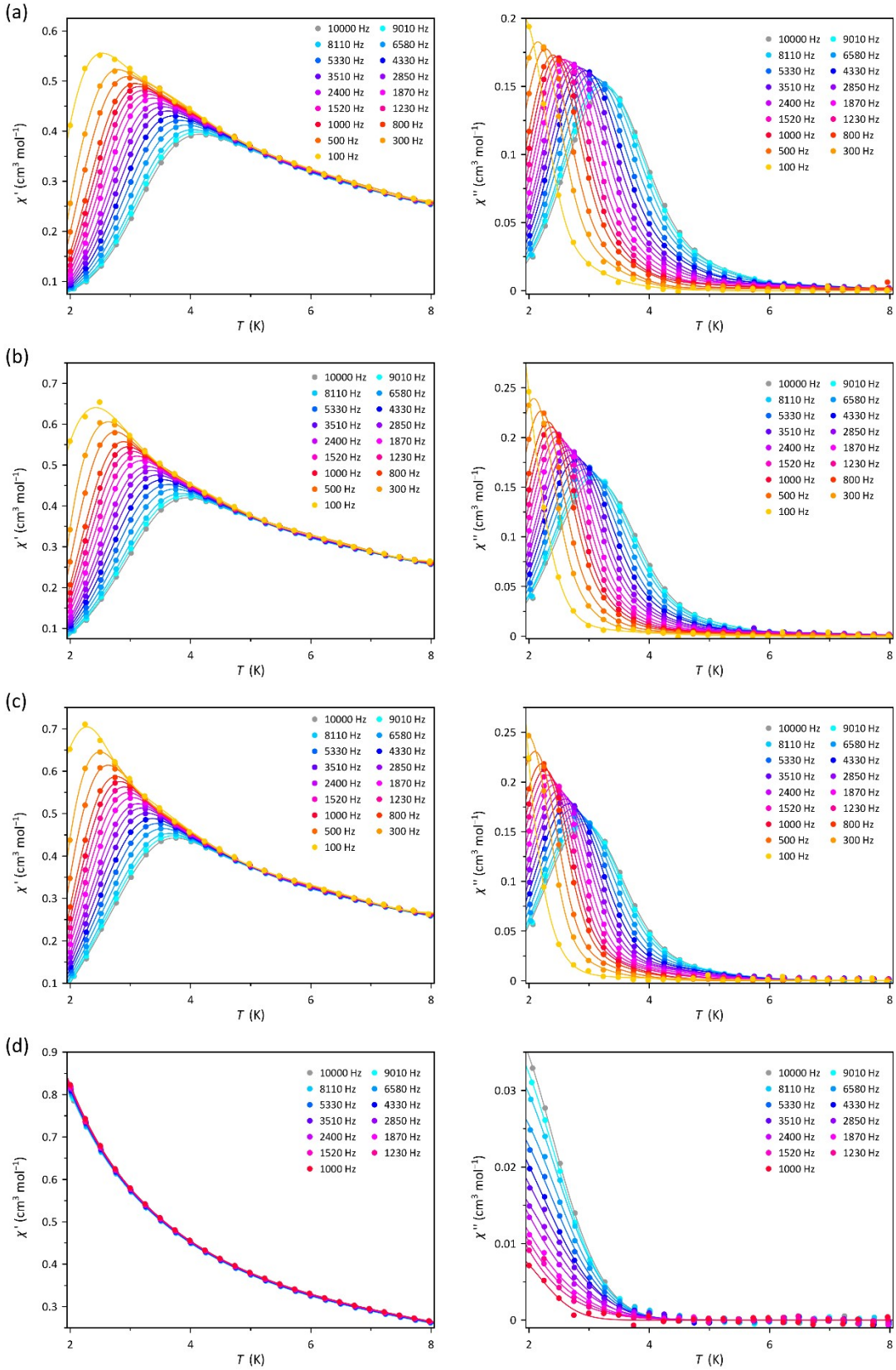

Figure S54. Temperature dependence of χ_M' (left) and χ_M'' (right) for **1** at a ±5.0 G oscillating field in the frequency range 0.3–10.0 kHz (gray to orange) under applied static magnetic fields of 2.5 (a), 1.0 (b), 0.5 (c) and 0 kOe (d). The solid lines are only eye-guides.

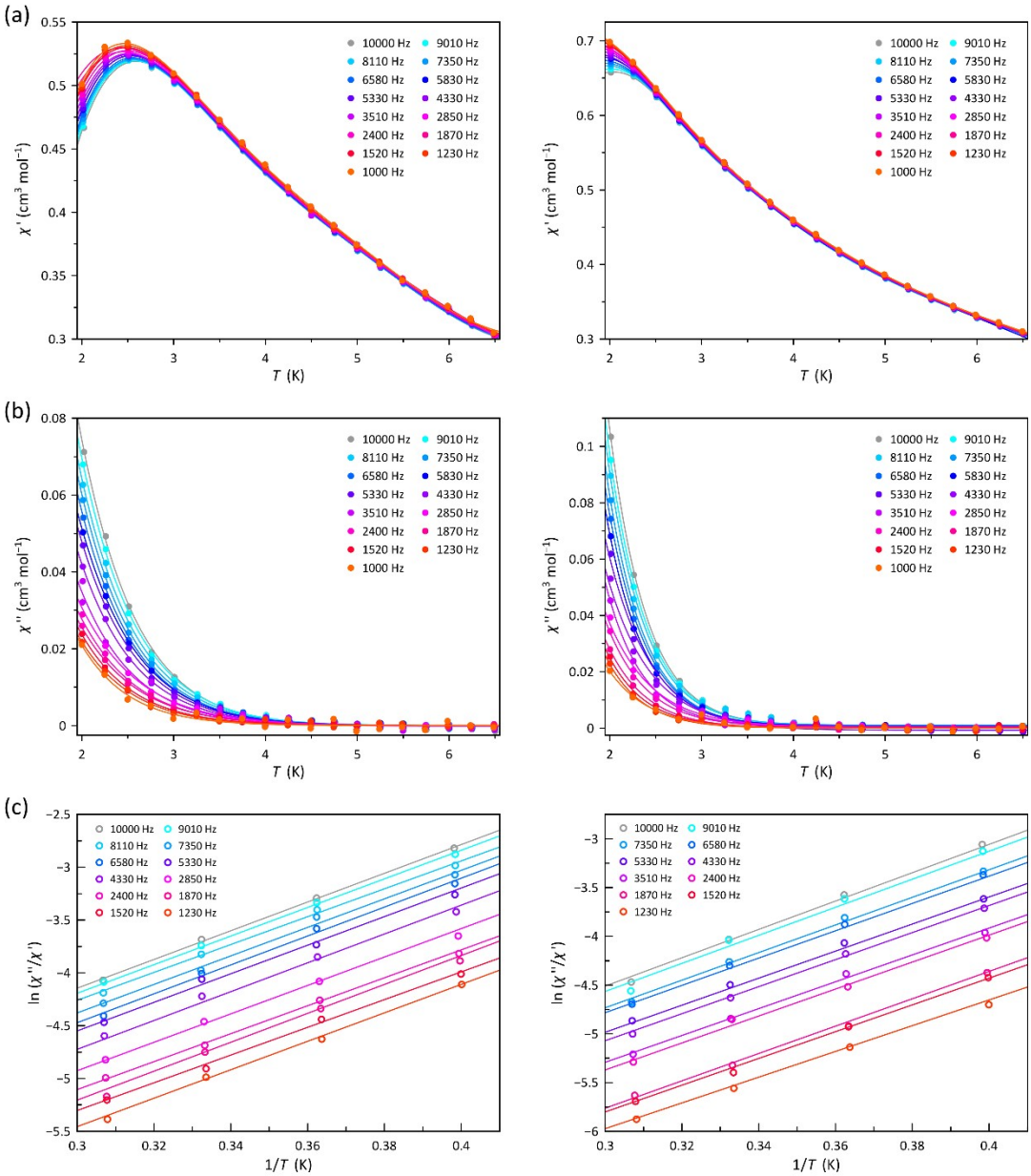

Figure S55. Temperature dependence of (a) χ_M', (b) χ_M'', and (c) $\ln(\chi_M''/\chi_M')$ for **2** at a ±5.0 G oscillating field in the frequency range 1.0–10.0 kHz (gray to orange) under applied static magnetic fields of 5.0 (left) and 2.5 kOe (right). The solid lines are only eye-guides.

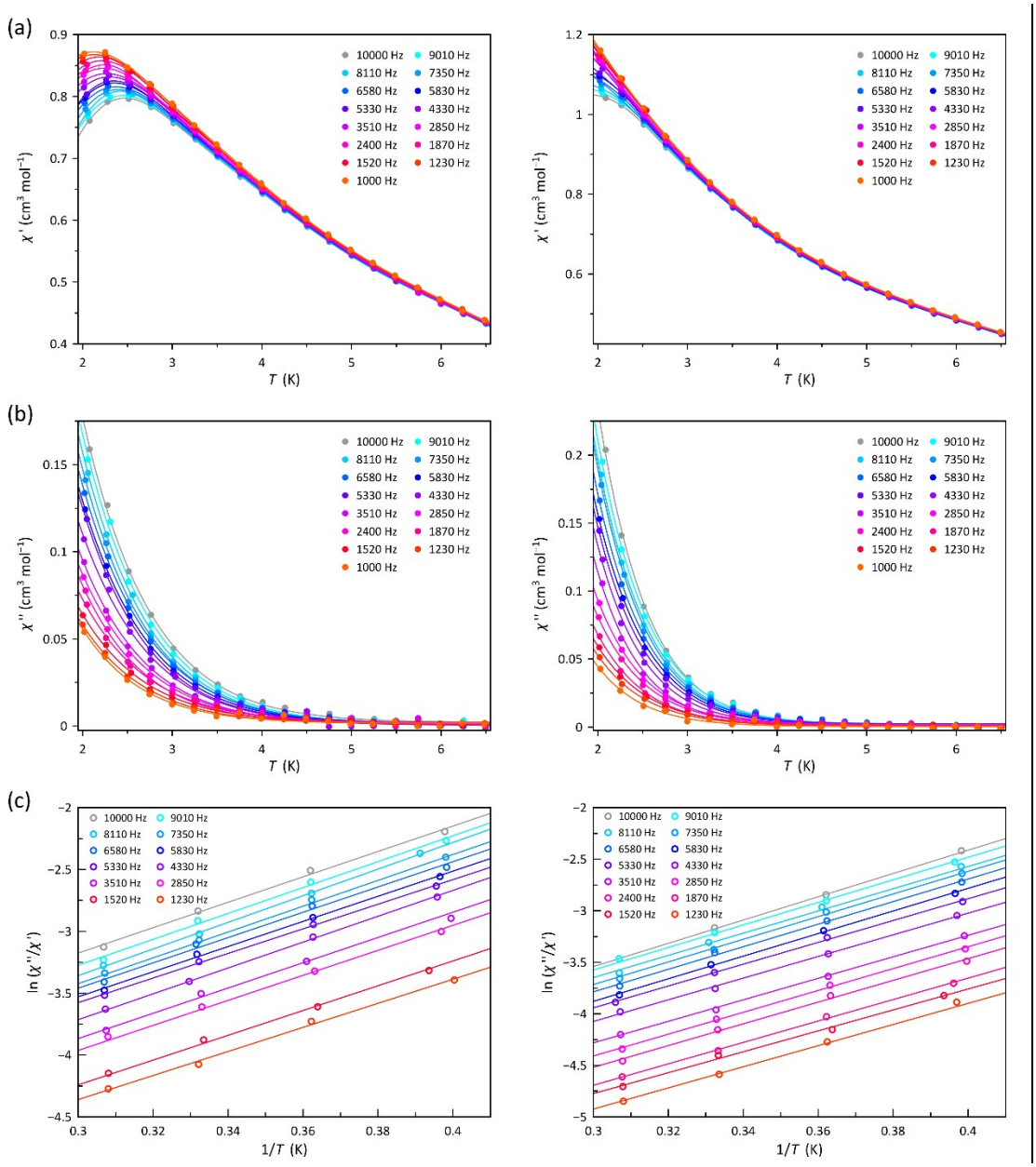

Figure S56. Temperature dependence of (a) χ_M', (b) χ_M'', and (c) $\ln(\chi_M''/\chi_M')$ for **3** at a ±5.0 G oscillating field in the frequency range 1.0–10.0 kHz (gray to orange) under applied static magnetic fields of 5.0 (left) and 2.5 kOe (right). The solid lines are only eye-guides.

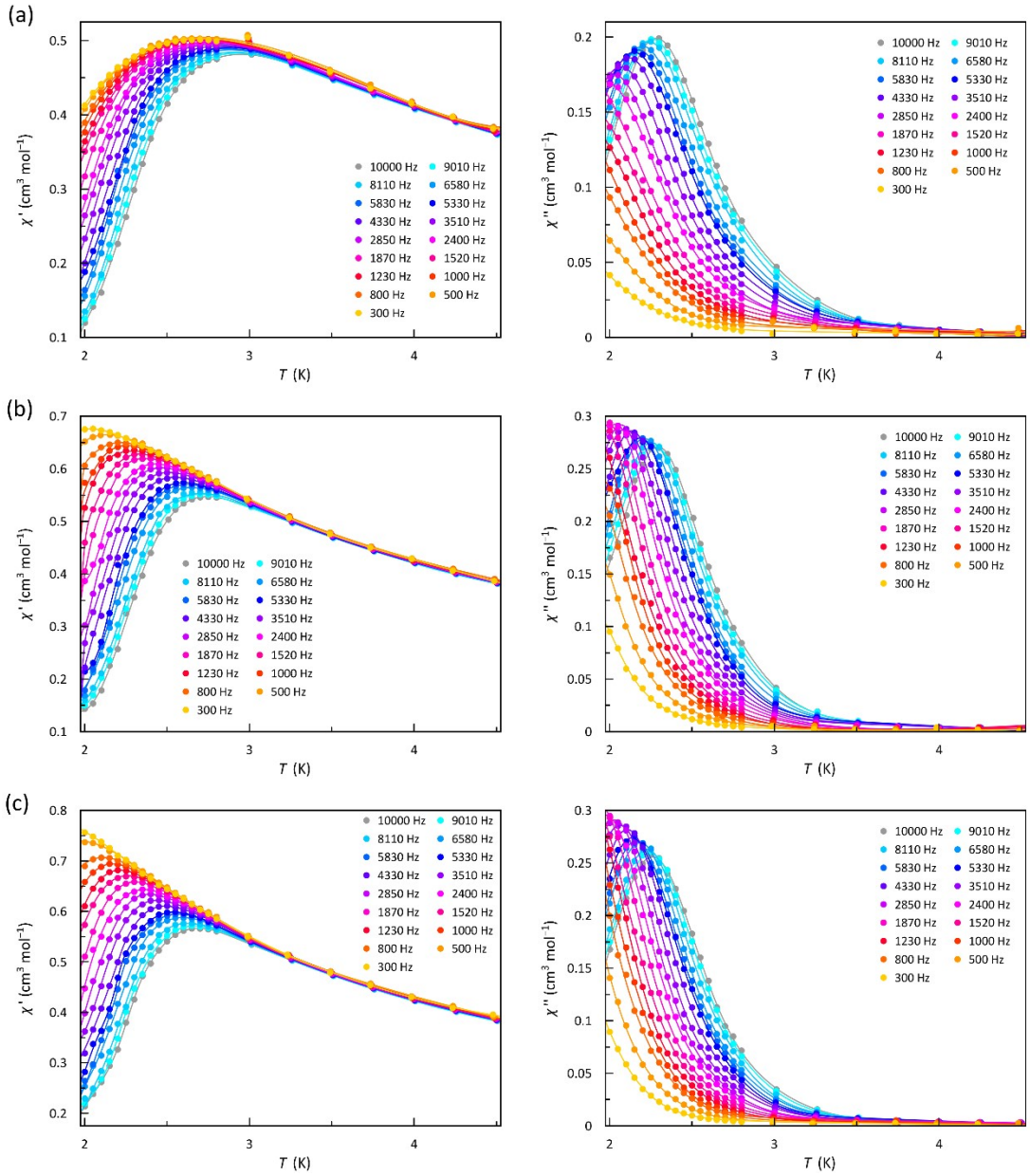

Figure S57. Temperature dependence of χ_M' (left) and χ_M'' (right) for **4** at a ±5.0 G oscillating field in the frequency range 0.3–10.0 kHz (gray to orange) under applied static magnetic fields of 2.5 (a), 1.0 (b) and 0.5 kOe (c). The solid lines are only eye-guides.

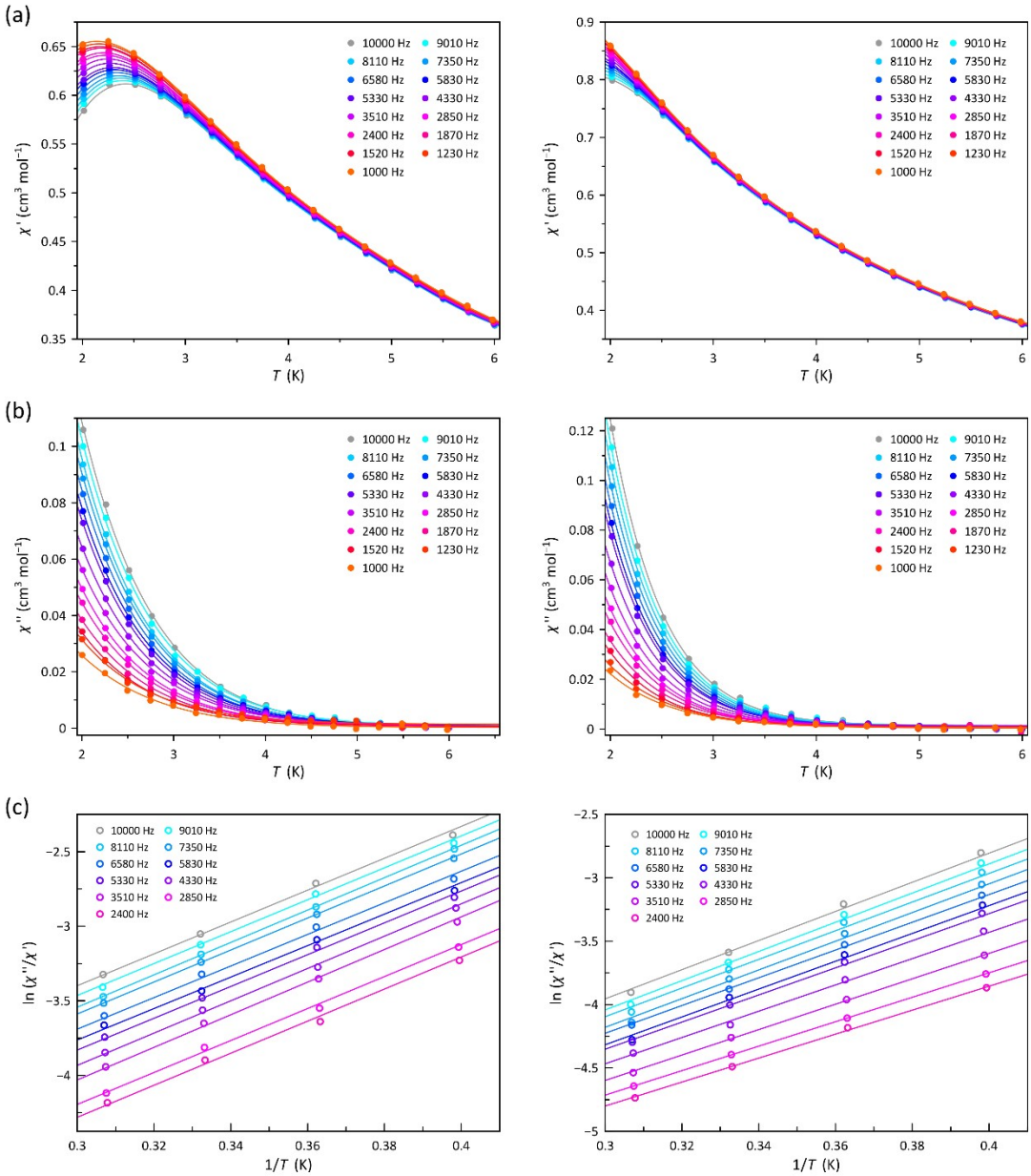

Figure S58. Temperature dependence of (a) χ_M', (b) χ_M'', and (c) $\ln(\chi_M''/\chi_M')$ for **5** at a ±5.0 G oscillating field in the frequency range 1.0–10.0 kHz (gray to orange) under applied static magnetic fields of 5.0 (left) and 2.5 kOe (right). The solid lines are only eye-guides.

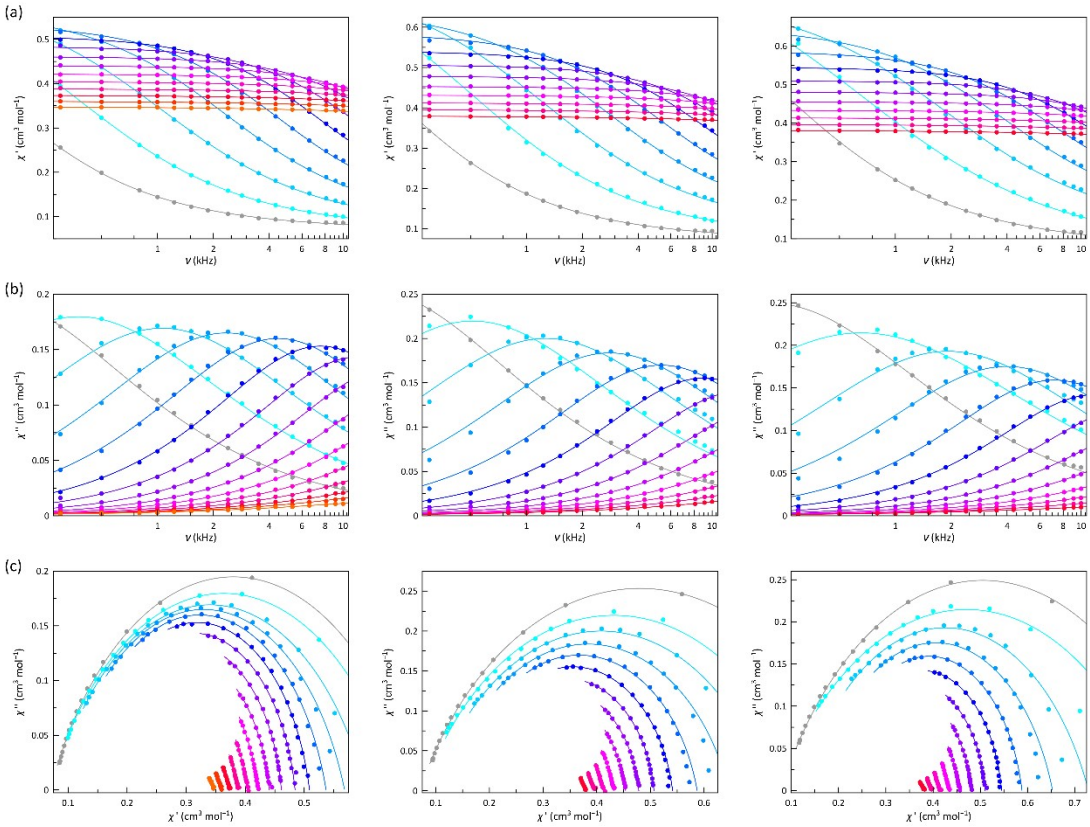

Figure S59. Frequency dependence of $\chi_{M'}$ (a), $\chi_{M''}$ (b) and Argand plots (c) for **1** under static magnetic fields of 2.5 (left), 1.0 (middle) and 0.5 (right) kOe with ±5.0 Oe oscillating field in the temperature range 2.0–5.5 K in steps of 0.25 K (from grey to orange). The solid lines are the best-fit curves simulated by using the generalised Debye model

1.9. ^{1}H NMR analysis of cycloaddition reactions

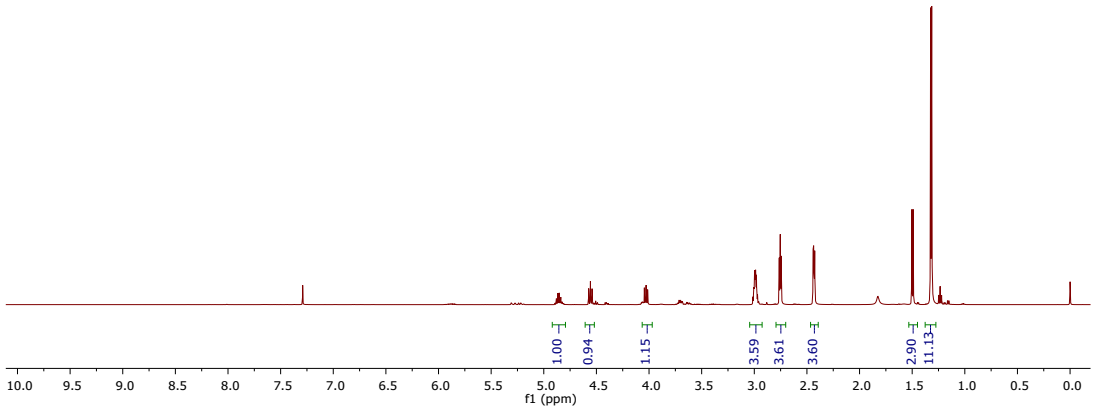

Figure S60. ^{1}H NMR of crude mixture of reaction using propylene oxide.

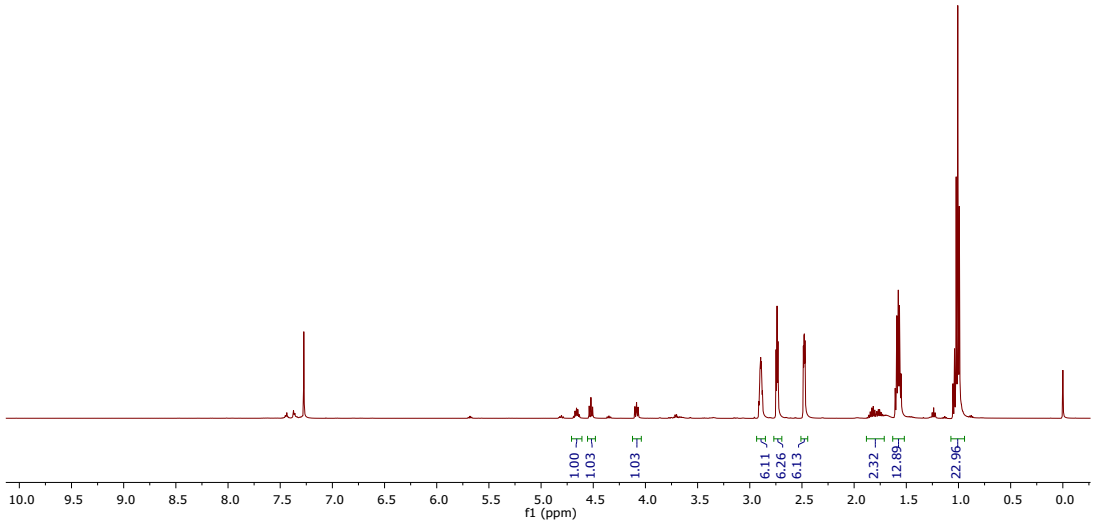

Figure S61. ^{1}H NMR of crude mixture of reaction using 2-butyloxirane.

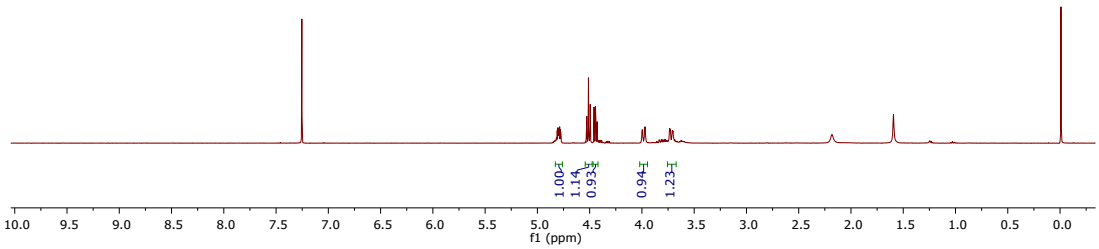

Figure S62. ^{1}H NMR of crude mixture of reaction using glycidol.

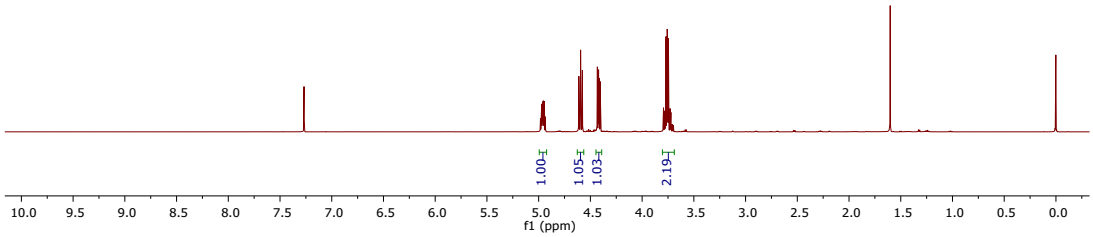

Figure S63. ^{1}H NMR of crude mixture of reaction using epichlorohydrin.

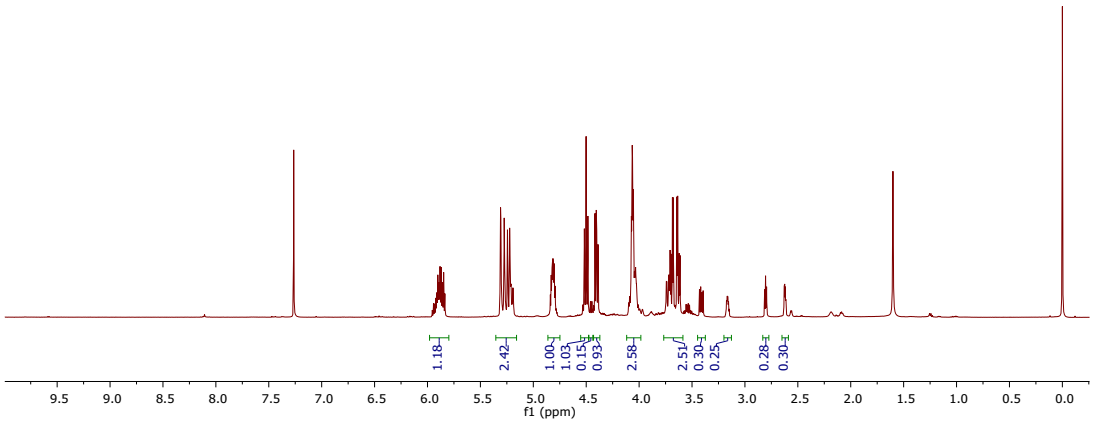

Figure S64. ^{1}H NMR of crude mixture of reaction using ally glycidyl.

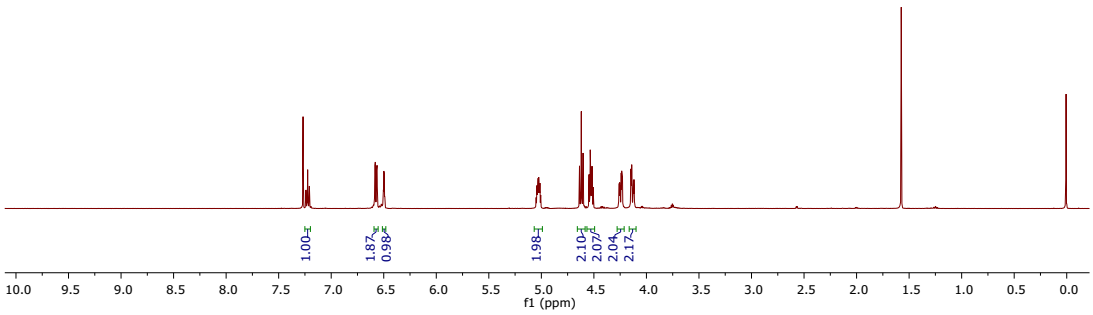

Figure S65. ^{1}H NMR of crude mixture of reaction using ally glycidyl ether.

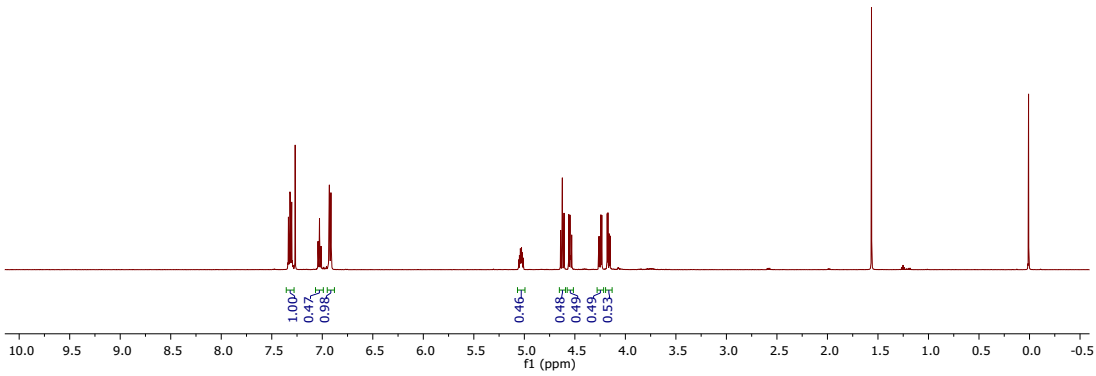

Figure S66. ^{1}H NMR of crude mixture of reaction using resorcinol diglycidyl ether.

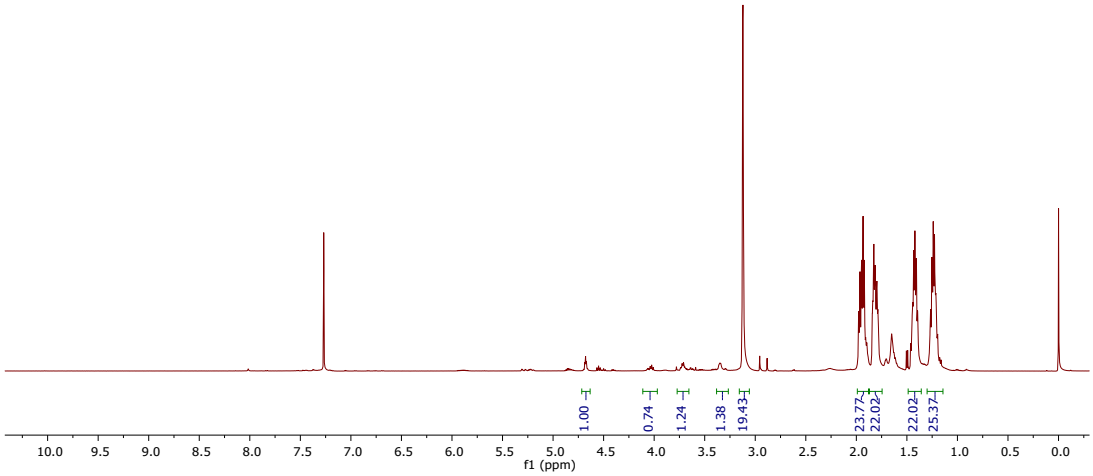

Figure S67. ^{1}H NMR of crude mixture of reaction using cycloexene oxide.